Int J Earth Sci (Geol Rundsch) (2004) 93:262–281
DOI 10.1007/s00531-004-0391-x

ORIGINAL PAPER

Dieter Mader · Franz Neubauer

Provenance of Palaeozoic sandstones from the Carnic Alps (Austria): petrographic and geochemical indicators

Received: 17 June 2002 / Accepted: 17 January 2004 / Published online: 20 March 2004
© Springer-Verlag 2004

Abstract An integrated approach of petrographic analysis, whole rock geochemistry and microprobe analysis has been applied to obtain information on the geodynamic development and the provenance for Ordovician to Permian siliciclastic successions exposed within the Carnic Alps (Austria). Sandstone detrital mode and geochemical results refine previous geodynamic interpretations. Late Ordovician samples indicate a stable craton and recycled orogenic and, possible, extensional setting. The Early Carboniferous is interpreted to represent a compressional environment, followed by a Late Carboniferous molasse-type foreland basin, and a Permian extensional geodynamic setting. Contrasting geochemical patterns of post-Variscan and Permian sequences suggest a rift setting. Electron microprobe data of detrital white mica also indicate changes in the provenance. Compositional data reflect a shift from low- to medium-grade metamorphic (Ordovician) to high-grade metamorphic (Carboniferous) to low- to medium-grade metamorphic and plutonic source rocks (Permian). Additionally, our data show that various chemical discrimination diagrams do not include all possible ranges of sandstones, and that high contents of detrital mica and ultra-stable heavy minerals may cause misclassification. Consequently, we propose the use of multi-method approach for provenance studies, including the control of geochemical data by modal analysis and heavy mineral investigations.

Keywords Detrital mica · Detrital mode · Palaeozoic · Sandstones · Southern Alps

D. Mader (✉) · F. Neubauer
Institut für Geologie und Paläontologie,
Paris Lodron Universität Salzburg,
Hellbrunnerstrasse 34, 5020 Salzburg, Austria
e-mail: a9010937@unet.univie.ac.at or franz.neubauer@sbg.ac.at
Fax: +43-662-8044621

Present address:
D. Mader, Institut für Geologische Wissenschaften,
Universität Wien,
Althanstrasse 14, 1090 Wien, Germany

Introduction

Clastic sedimentary rocks are indicators for past environments, giving clues to their composition and even to their geodynamic setting by means of their components. The provenance and geodynamic development of sandstone successions can be classified by a variety of methods, including petrographic analysis, whole rock and mineral chemistry, and radiometric dating. Above all, clastic sediments can supply information on continental and oceanic source regions that have been eroded or metamorphosed through subsequent tectonic processes. In siliciclastic rocks, some detrital minerals are characteristic for certain source rocks and source regions. Thus, often only the detrital components of clastic rocks reveal clues to areas that have disappeared.

On a volumetric basis, values of detrital framework minerals can classify siliciclastic rocks and indicate their provenance (e.g. Crook 1974; Schwab 1975; Dickinson and Suczek 1979; Dickinson et al. 1983; Valloni and Dickinson 1984; Dickinson 1985). It is generally supposed that the detrital composition mostly depends on the composition of the source area and its tectonic setting, besides other factors such as climate, relief, distance of transport and diagenesis (Pettijohn et al. 1987; Johnsson 1993; McLennan et al. 1993; Fralick and Kronberg 1997, with references therein). After Ingersoll et al. (1984), the Gazzi–Dickinson method is suited best by reducing effects of grain size and secondary alteration.

Geochemical data can supply valuable information about the sedimentary processes such as weathering, transport, diagenesis and, due to the role of tectonism as a primary control on the composition of sediments, geochemical analyses may be used to identify the source area and tectonic setting of the depositional basins (e.g. Pettijohn et al. 1972; Blatt et al. 1980; Taylor and McLennan 1985; Argast and Donnelly 1987; McLennan et al. 1990, 1993; Floyd et al. 1991; Johnsson 1993; Zhang et al. 1998; Bauluz et al. 2000). However, the composition of rocks and the composition of the source area do not correlate entirely, as weathering in the source

region may have led to compositional changes (e.g. Nesbitt 1979; McLennan 1989).

Due to the abundance of fossils, the structurally relatively undisturbed late Middle Ordovician to Permian sequences, and the very low-grade (Variscan and Alpine) metamorphic overprint, the Carnic Alps have become a classical area for stratigraphic investigations of Palaeozoic formations (e.g. Schönlaub 1985a; Schönlaub and Histon 2000). However, mainly fossil-rich carbonate sequences have been studied, and little attention has been paid to the siliciclastic formations, which can be generally found near the base and top of the lithostratigraphic section in the Carnic Alps. Consequently, no integrated petrographic, geochemical and isotopic studies on terrigenous sediments in the Carnic Alps have been performed. Previous studies on provenance and of the sedimentary facies in the Carnic Alps based on heavy mineral analyses proposed the basement of the Carnic Alps or the Gailtal basement as source areas (e.g. Tietz 1974; Schnabel 1976; Fenninger and Stattegger 1977). Sedimentary, petrographic and/or geochemical studies on siliciclastic sedimentary rocks of this region have been reported by Fontana and Venturini (1982), Spalletta and Venturini (1988), Venturini (1990a, with references), Hinderer (1992), Krainer (1992), Läufer et al. (1993), Poscheschnik (1993) and Neubauer (1994). Based on $^{40}Ar/^{39}Ar$-dating of detrital white mica, Dallmeyer and Neubauer (1994) proposed a Cadomian hinterland for Late Ordovician clastic sequences of the Carnic Alps, and this interpretation was recently confirmed by Pb/Pb evaporation ages on zircons (Neubauer et al. 2001).

The present study uses petrographic and geochemical methods on Ordovician to Permian sandstones to evaluate current geodynamic models for the evolution of the Carnic Alps. The main objective is to show the geologic significance and provenance of sandstones within different types of Ordovician to Permian sedimentary basins, including an Early Carboniferous syn-orogenic flysch trough, Late Carboniferous post-orogenic molasse and Permian rift basins. The main emphasis has been taken on the Carboniferous formations, specifically as $^{40}Ar/^{39}Ar$ dating using the same samples (Mader et al. 2000) displayed entirely different source regions between Early and Late Carboniferous successions (see below). The study also aims to assess petrographic and geochemical methods using sandstones for discrimination of geodynamic settings.

Geologic setting

The study area is located in the central Carnic Alps (Carinthia, Austria) near the border to Italy (Fig. 1). The Carnic Alps comprise the sedimentary basement of the Southern Alps, and are exposed in their north-eastern part, adjacent to and separated from the Austroalpine units by the Periadriatic lineament (Fig. 1). Tollmann (1985), Schönlaub (1985a), Schönlaub and Histon (2000) and Läufer et al. (2001) reviewed the research of this area.

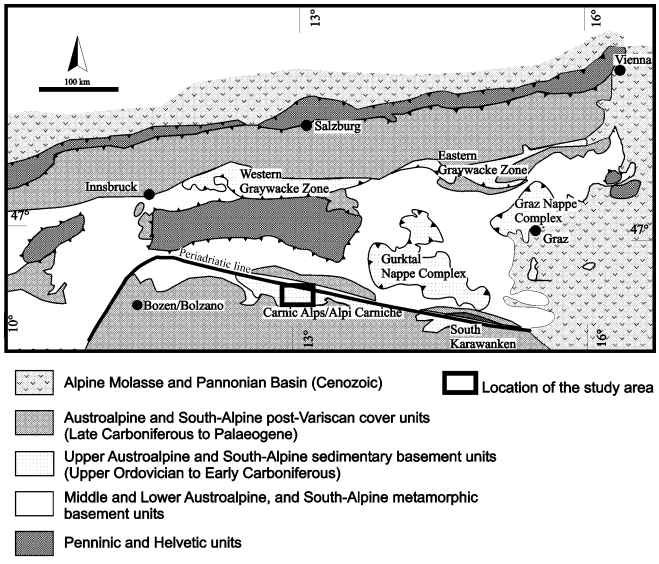

Fig. 1 Schematic geologic map of the Eastern Alps

The central Carnic Alps, together with the Greywacke zone, and the southern Karawanken Alps, which both show lithologic similarities to the Carnic Alps, and the Gurktal and Graz Palaeozoic successions, are considered as the southern external zone of the European Variscides, analogous to the Rhenohercynic and Saxothuringic zones, which represent the northern external zone of the European Variscides (e.g. Franke 1989; Schönlaub and Heinisch 1993; von Raumer 1998; Stampfli et al. 2002).

The Carnic Alps are characterized by a continuous, fossiliferous, non- to low-grade metamorphosed sedimentary sequence that can be divided into two major successions (Fig. 2). The older, a pre-Variscan group, comprises Late Ordovician to early Late Carboniferous sequences, which are overlain by a post-Variscan cover. Both successions are separated by an angular unconformity that formed at the Westphalian C/D boundary (e.g. Fenninger et al. 1976; Schönlaub 1985a; Schönlaub and Heinisch 1993, with references therein).

The stratigraphic record starts with thick late Middle and Late Ordovician volcanic and subsequent marine siliciclastic and minor carbonate shallow-water deposits (e.g. Schönlaub and Heinisch 1993; Läufer et al. 2001). These are overlain by Silurian to Early Devonian black shales (Bischofalm facies), thick shallow marine platform carbonates, pelagic limestones and siliciclastic sediments, which, collectively, indicate a basin-and-swell facies near a passive continental margin (Schönlaub and Heinisch 1993). The Bischofalm facies realm is strongly deviating from other facies realms, although facies transitions are known because of its low thickness (<200 m for Silurian and Devonian) and the dominance of black, partly graptolite-bearing shales, which are intercalated by cherts, thin limestones and rare sandstone layers. From Late Devonian to Early Carboniferous, pelagic limestones and cherts ('lydites') suggest either initial rifting or relative sea level rise. Visean–Namurian flysch deposits, with

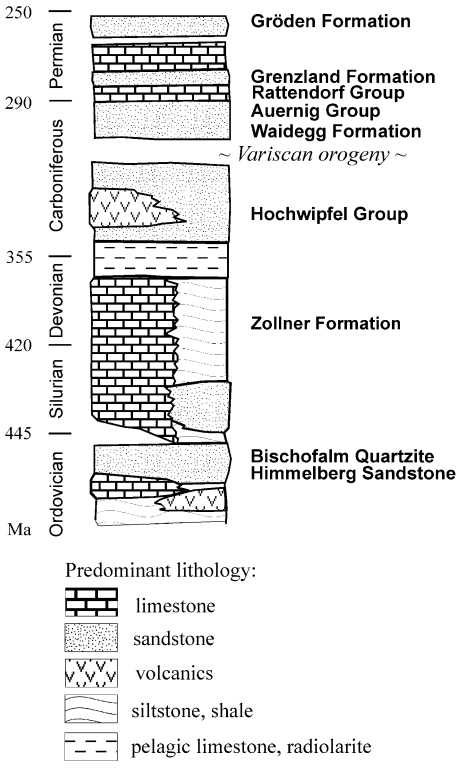

Fig. 2 Schematic stratigraphic section of the Palaeozoic units in the Carnic Alps with emphasis on the siliciclastic sequences (strongly simplified after Schönlaub and Heinisch 1993)

turbidites and interbedded olisthostromes, indicate the onset of the Variscan orogeny (Spalletta and Venturini 1988; Neubauer and Handler 2000; Läufer et al. 2001, and references therein). From Late Namurian to Early Westphalian (Bashkirian to Moscovian), the Carnic Alps were uplifted and eroded for a period not exceeding 5 Ma (Flügel 1975; Spalletta et al. 1980). Above a well-defined angular unconformity (Fenninger et al. 1976), Late Carboniferous molasse deposits with cyclic shallow marine carbonates and sandstones to terrestrial conglomerates (Auernig Group) grade into Permian terrestrial red-beds and shallow-marine carbonate and siliciclastic sediments of the South-Alpine Permian to Triassic succession (e.g. Krainer 1993).

Samples were taken from sandstone-bearing units through the Palaeozoic sequences in the central Carnic Alps (Fig. 3). In order to facilitate comparisons based on currently available geodynamic evidence (Krainer 1993; Neubauer and Sassi 1993; Schönlaub and Heinisch 1993; Schönlaub and Histon 2000; Läufer et al. 2001), these samples were grouped into (1) Late Ordovician and Devonian extensional environments (Ordovician Himmelberg Sandstone and Bischofalm Quartzite, and the peculiar euxinic, pelagic Devonian Bischofalm facies with a single sample of the Zollner Formation); (2) Early Carboniferous contractional environments, as represented by syn-orogenic flysch formations (Hochwipfel Group); (3) Late Carboniferous molasse (Waidegg Formation, Auernig Group); and (4) Permian extensional environments caused by ongoing post-Variscan rifting (Grenzland and Gröden Formations).

Sandstone samples are the same as used for $^{40}Ar/^{39}Ar$ dating of detrital white mica in a companion study (Mader et al. 2000). Early Variscan (Devonian) ages (373–396 Ma) were found within Early Carboniferous sandstones, and Variscan ages (333–309 Ma) in Late Carboniferous and Permian sandstones.

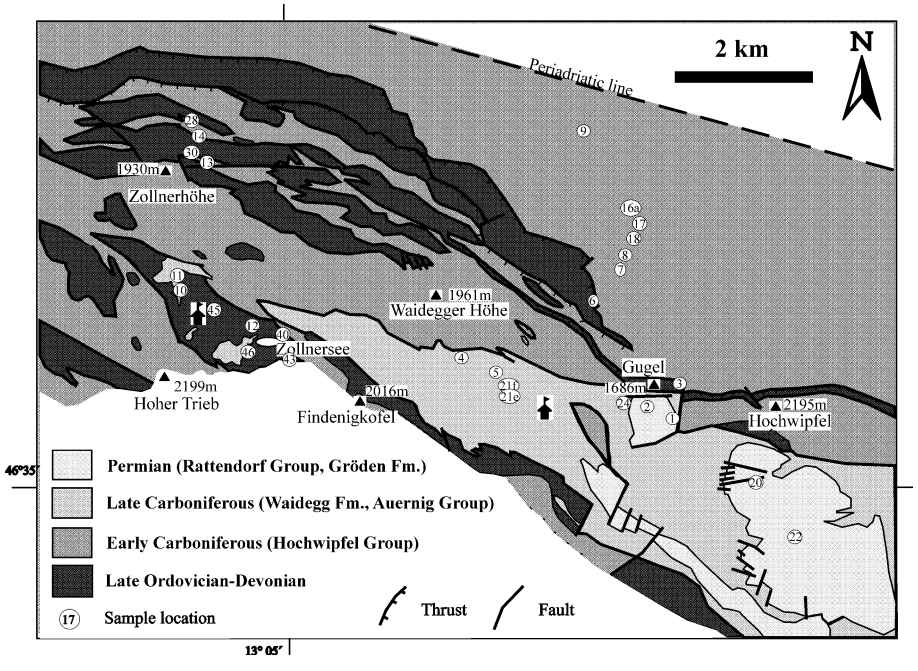

Fig. 3 Detailed map of the study area with sample locations (modified after Schönlaub 1985b, 1987). Sample 15 (from the Hochwipfel Group) is located outside of the figure (to the east)

Analytical methods

Samples are from massive interiors of sandstone beds, except sample DM12 (Late Ordovician, DM45 (Devonian) and DM1 (Permian), which are laminated very fine-grained sandstones/siltstones. A total of 24 medium- to fine-grained, Ordovician, mainly Carboniferous, and Permian samples were point-counted for detrital mode analysis with a semi-automatic Swift Point-Counter (Table 1). Depending on groundmass content, 350–500 framework grains were counted. All components below 0.063 mm apparent diameter (silt and clay fraction) were counted as matrix, as well as cement crystals regardless of size. Sand-sized subgrains of polycrystalline quartz, feldspar and rock fragments were counted as monocrystalline quartz and feldspar, following the Gazzi–Dickinson method (e.g. Dickinson and Suczek 1979; Ingersoll et al. 1984). According to the Gazzi–Dickinson method, we distinguish between the following framework constituents: monocrystalline quartz (Qm), polycrystalline quartz (Qp), feldspar (F) comprising plagioclase (P) and K-feldspar (K), lithic volcanic (Lv) and lithic sedimentary clasts (Ls), white mica, biotite and heavy minerals. Heavy minerals include opaque and translucent grains.

In addition, translucent heavy mineral contents (ca. 150–300 grains) were counted in 17 thin sections (Table 2). The same area was used for counting in all sections, with equal distances between profile lines and the same magnification. All transparent heavy minerals (>20 μm; rutile, zircon, garnet, apatite, tourmaline) observed in the ocular were counted because heavy minerals are rather small (<100 μm) in thin sections, and the principal goal of heavy mineral investigations was to reveal the cause for anomalies in the chemical composition of sandstones (see below).

For whole rock geochemical analysis, 18 medium- to fine-grained, Late Ordovician to Permian sandstones were cleaned, crushed and pulverized in an agate mill. The major and trace element compositions were determined in the Centre de Recherches Petrographiques et Geochimiques (at CNRS) in Vandoeuvre les Nancy (France) by ICP-AES for major and minor elements, and ICP-MS for trace elements. Samples were fused there with $LiBO_2$ and HNO_3 dissolution prior to analysis. Quality was controlled by comparison with international geostandards. Results are shown in Tables 3 and 4.

White mica concentrates for microprobe analysis (and $^{40}Ar/^{39}Ar$ dating of the companion study) were prepared from sieve fraction 0.125–0.200 mm by flotation in water columns, purification by dry-sieving and separation by a Frantz isodynamic magnetic separator. This leads to an enrichment of mica grains with distinct chemical compositions, which are mostly enriched in phengite and/or paragonite contents due to magnetic separation. Finally, mica grains were hand selected under a binocular microscope, and polished multigrain sections were prepared from seven concentrates of detrital white mica (Permian samples: DM2, 22, Carboniferous samples: DM4, 9, 14, Ordovician samples: DM3, 12). Sample DM3 represents the entire fraction (without concentration by magnetic separation) because of the scarcity of mica. Additionally, detrital micas were analysed in six, mainly Carboniferous, thin sections (DM2, 5, 21e, 9, 13, 17). Microprobe analyses were carried out on a JEOL electron microprobe (JXA-8600) at the Institute of Geology and Palaeontology, University of Salzburg, using a wavelength dispersive system, an accelerating voltage of 15 kV and a sample current of 40 nA. The electron beam was focused to 5 μm. Natural and synthetic mineral-oxide standards were used. Standard ZAF correction calculations led to the chemical composition of the micas. Two or three spots on individual mica grains per specimen were measured for quantitative chemical determination (results are given in Table 6).

Results

Detrital modes

Triangular diagrams of detrital mode analyses are usually applied for the classification of sandstones, using the three detrital framework components quartz, feldspar and rock fragments (e.g. Williams et al. 1953; McBride 1963; Dott 1964; Pettijohn et al. 1972). Depending on the matrix content, two triangular graphs are in use, one for matrix-rich wackes (>15% matrix) and another one for matrix-poor arenites (<15% matrix; Dott 1964; Pettijohn et al. 1972). In those graphs, chert grains are dedicated to the lithic corner. Because in this study the Gazzi–Dickinson method was applied, the Q_mFL_t plot was selected for the sandstone classification.

Eight samples, mainly Early Permian and Late Carboniferous, can be displayed in the triangular diagram for matrix-poor arenites due to their matrix content of less than 15%. Quartz dominates the distribution, whereas feldspar and rock fragments are fairly rare. Hence, these samples plot as lithic arenites or sublitharenites (Fig. 4).

The remaining samples must be plotted in the triangular diagram for wackes because of their matrix content >15% (24.6–57.2%, but note that matrix is generally regarded as material smaller than 30 μm). In this study all grains consisting of a grain size between 30–60 μm (silt) were counted as matrix (Fig. 4). The relatively larger amount of feldspar and rock fragments depict these samples, represented by the Ordovician, Early Carboniferous, some Late Carboniferous (DM15, DM21e) and Late Permian, as lithic greywacke and quartz wacke.

All samples show a phyllosilicatic matrix, but few additionally contain some carbonatic cement. The Late Ordovician samples contain, beside silt-sized quartz grains, a matrix of sericite and clay and, possibly, few grains of pseudomatrix derived from unstable lithic components. Some thin sections bear limonite or/and haematite in pressure solution bands or as shapeless aggregates. One thin section of the Late Ordovician Bischofalm Quartzite (DM6) displays carbonate cement. The cementing solution might have dissolved feldspars as

Table 1 Modal abundances (%) of Palaeozoic sandstones from the Carnic Alps. *Q* Quartz; *F* feldspar; *L* lithic fragments; *Lt* lithic fragments and polycrystalline quartz; *Qm* monocrystalline quartz; *Qp* polycrystalline quartz; *K* K-feldspar; *P* plagioclase; *Ls* sedimentary lithic clast; *Lv* volcanic lithic clast; *Lm* metamorphic lithic clast; *M* detrital white mica; *HM* heavy minerals; *GM* matrix and cement; *GD* Gröden/Val Gardena Formation; *GL* Grenzland Formation; *AG* Auernig Group; *WD* Waidegg Formation; *HW* Hochwipfel Group; *BA* Bischofalm Quartzite; *HB* Himmelberg Sandstone

Sample		Q	F	L	Lt	Qm	Qp	K	P	Ls	Lv	Lm	M	HM	GM	Sum
DM2	GD	67.6	15.8	7	34.2	40.4	27.2	12.8	3	4	2.2	0.8	9.2	0.4	31.9	100
DM20	GL	91.4	0	0	11.4	80	11.4	0	0	0	0	0	8	0.6	7.9	100
DM22	GL	75.9	0.5	18.2	27.6	66.5	9.4	0.5	0	5.4	0	12.8	3.4	0.8	8.9	98.8
DM4	AG	90.4	0	1.4	11.6	80.2	10.2	0	0	1.4	0	0	6	2	5.4	99.8
DM5	AG	84.9	0	1.4	12.6	73.7	11.2	0	0	0.7	0.5	0.2	11.2	2.2	11.7	99.7
DM15	AG	79.1	0	0	21.4	57.7	21.4	0	0	0	0	0	18.8	2	36.7	99.9
DM21e	AG	75.1	0	0.5	4.2	71.4	3.7	0	0	0.5	0	0	22.2	2	48.1	99.8
DM21f	AG	87.1	0	0.5	16.2	71.4	15.7	0	0	0.5	0	0	9.4	2.8	8.1	99.8
DM24	AG	94.2	0	5	43.2	56	38.2	0	0	4.2	0	0.8	0.2	0.2	3	99.6
DM11	WD	86.5	0	1	14.4	73.1	13.4	0	0	0.5	0	0.5	10.6	1.7	12.9	99.8
DM46	WD	87.6	0	2.5	26.7	63.4	24.2	0	0	0.5	0	2	8	1.7	17.1	99.8
DM7	HW	54.4	9.6	35.8	54.8	35.4	19	5	4.6	24.2	5.8	5.8	0.2	0	38.1	100
DM8	HW	69.8	15	10.2	20.6	59.4	10.4	8	7	5.4	0.6	4.2	4.6	0.4	55.9	100
DM9	HW	55.4	19.4	19.4	32.8	42	13.4	14.8	4.6	8.8	3.6	7	3.6	2.2	53.6	100
DM13	HW	72	9.4	16	30.4	57.6	14.4	3.4	6	8	4	4	2	0.6	51.3	100
DM16a	HW	76.6	13.8	5.8	23.2	59.2	17.4	9.2	4.6	1.2	0	4.6	2.8	1	57.2	100
DM17	HW	62.6	18.6	17.6	37.6	42.6	20	11.6	7	8.6	2	7	0.6	0.3	48.7	99.7
DM18	HW	64	9	21	30.4	54.6	9.4	3.8	5.2	14.6	2.4	4	4.4	1.6	47	100
DM28	HW	81.8	3.8	12.6	34.4	60	21.8	2.2	1.6	9.4	1.2	2	1.2	0.6	33.3	100
DM30	HW	79.8	6.4	13.2	34.4	58.6	21.2	3.2	3.2	7.8	3.4	2	0	0.6	36	100
DM3	BA	96.3	2.1	0.8	5.1	92	4.3	1.3	0.8	0.8	0	0	0.3	0.8	30.2	100
DM6	BA	99.3	0.2	0	2.2	97.1	2.2	0.2	0	0	0	0	0	0.2	56.4	99.7
DM43	BA	97.4	1.1	0	21.4	76	21.4	1.1	0	0	0	0	0	1.4	30.6	99.9
DM40	HB	97.2	2	0.2	10.8	86.6	10.6	1.4	0.6	0.2	0	0	0	0.6	24.6	100

Table 2 Mean values (rel % of grains) of translucent heavy minerals from sandstones from the Carnic Alps. *n* Number of samples

	Permian	Late Carboniferous	Early Carboniferous	Ordovician
n	3	5	5	4
Rutile	46.7	73.5	35.7	29.4
Tourmaline	28.0	16.5	9.0	30.6
Zircon	24.7	9.9	32.1	37.4
Apatite	0.0	0.1	6.0	1.7
Garnet	0.6	0.0	17.2	0.9

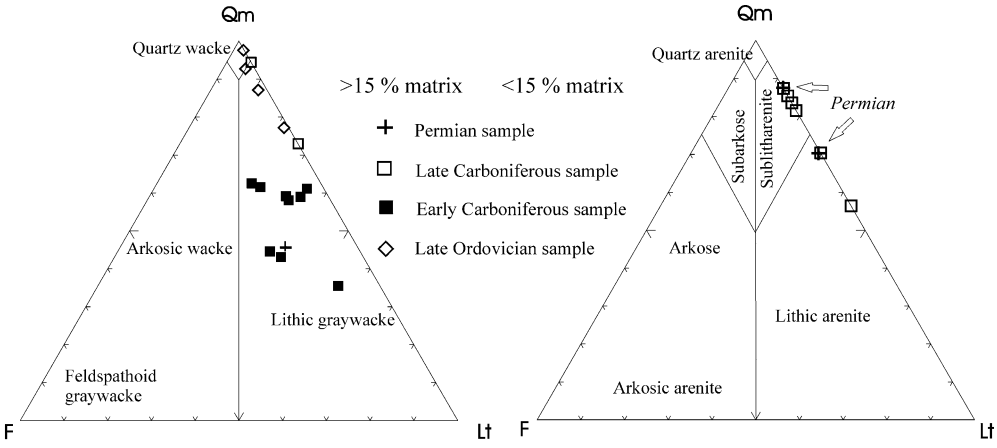

Fig. 4 Sandstone classification diagram (after Pettijohn et al. 1972). Instead of the QFL graph the Q_mFL_t graph was used due to different interpretation of Q and L by the classification diagram after Pettijohn et al. (1972) and the provenance diagram after the Gazzi–Dickinson method

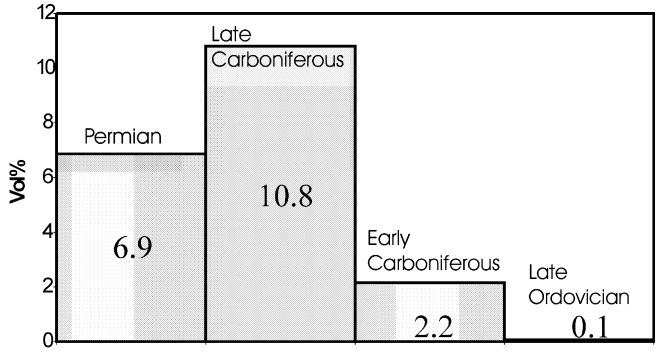

Fig. 5 Histogram of the relative proportion of white mica within framework components of Late Ordovician to Permian sandstones

indicated by a few nearly completely dissolved feldspar grains. The matrix of the Early Carboniferous samples is composed of chlorite, sericite, quartz silt, clay and goethite(?). Some pseudomatrix of lithic components may occur. In some thin sections (DM9, 17), carbonate cement occurs in addition to the siliciclastic matrix. The matrix of the Late Carboniferous samples is composed of silt-sized quartz, chlorite, clay, sericite and limonite, the latter along some grain boundaries. The Permian samples contain a matrix of sericite, aggregates of hematite and clay. One Early Permian sample (DM20) contains patchy carbonate cement and even some euhedral rhomboeders of carbonate, likely siderite. A Late Permian sample (DM1) also shows carbonate cement.

High white mica contents, up to 22%, were found in Late Carboniferous sandstones, an important fact to be considered when interpreting detrital mode and geochemistry. Figure 5 shows the average white mica content of the different groups of samples. Partly chloritized biotite is present in samples from the Early Carboniferous in small proportions. Furthermore, matrix-sized biotite occurs in samples DM12 (Late Ordovician) and DM45 (Devonian).

In the QFL ternary provenance diagram (e.g. Dickinson and Suczek 1979; Dickinson et al. 1983), the quartz-rich sandstones of the Ordovician (Bischofalm Quartzite), the Late Carboniferous (Auernig Group) and the Early Permian (Grenzland Formation) plot into the continental block field (craton interior as subfield for quartz-rich compositions; Fig. 6a). In the Q_mFL_t diagram, however, due to the polycrystalline quartz grains, they mainly plot into the recycled orogenic source field (Fig. 6b). The greywackes and litharenites of the Early Carboniferous (Hochwipfel Group) and the Late Permian (Gröden Formation) plot into the recycled orogenic source field in both diagrams. In the $Q_pL_vL_s$ diagram (Fig. 6c), most of these samples point to collision suture and fold-thrust belt sources due to significant proportions of lithic fragments. Figure 6d shows, due to the scarcity of feldspars, mainly Early Carboniferous samples, which are displayed as derived from a mature continental block source.

In Late Ordovician sandstones, shale is the most important type of lithic fragments. Early Carboniferous sandstones include abundant sedimentary and metasedimentary fragments, including greywackes, phyllite, quartz-mica schists, shales and siltstones, and aphanitic, porphyric and sphaerolithic volcanic rocks. In Late Carboniferous sandstones, siltstone, mudstone and phyllite clasts largely predominate over a few volcanic

Table 3 Chemical composition of sandstones of the Carnic Alps. Major element oxides obtained by ICP-AES, respectively, ICP-MS. *AG* Auernig Group; *BA* Bischofalm Quartzite; *GD* Gröden Formation; *GL* Grenzland Formation; *HB* Himmelberg Sandstone; *HW* Hochwipfel Group; *WD* Waidegg Formation; *ZF* Zollner Formation; *tr.* traces

%	DM1	DM20	DM22	DM4	DM5	DM15	DM10	DM11	DM14	DM12	DM2	DM21e	DM9	DM13	DM17	DM45	DM3	DM40
	GD	GL	GL	AG	AG	AG	WD	WD	HW	HB	GD	AG	HW	HW	HW	ZF	BA	HB
SiO_2	46.38	85.62	79.63	89.25	85.44	75.15	66.44	81.55	72.11	52.48	72.03	60.92	64.67	76.27	66.35	63.7	89.56	89.17
Al_2O_3	15.98	5.58	10.84	6.42	8.46	13.04	12.84	8.83	14.15	21.02	14.62	20.85	15.28	10.74	11.29	14.79	4.51	4.71
Fe_2O_3	5.59	1.80	2.85	1.04	0.81	3.02	6.65	3.12	3.92	9.97	3.45	4.92	6.83	4.15	5.40	8.24	1.43	2.03
MnO	0.06	tr.	tr.	tr.	tr.	0.02	0.19	0.03	0.02	0.02	tr.	0.04	0.09	0.05	0.17	0.14	0.02	0.03
MgO	6.01	0.56	0.95	0.12	0.15	0.86	1.48	0.67	1.28	2.99	0.86	1.33	2.58	1.31	1.8	2.21	0.3	0.33
CaO	6.49	0.6	0.03	tr.	tr.	0.07	2.18	tr.	0.19	0.12	0.14	0.02	1.07	0.34	4.24	0.32	0.13	0.03
Na_2O	1.07	0.1	0.93	0.35	0.14	0.28	0.39	0.23	3.11	1.87	1.82	0.46	2.3	2.16	2.38	1.71	0.47	1.17
K_2O	4.64	0.86	2.14	1.19	1.44	2.48	2.35	1.55	2.1	4.54	3.37	3.77	2.54	1.55	1.35	2.76	1.07	0.72
TiO_2	0.54	0.33	0.51	0.37	1.3	1.13	0.93	1.16	0.73	1.06	0.56	1.02	0.93	0.56	0.68	2.1	0.35	0.39
P_2O_5	0.13	0.02	0.06	tr.	tr.	0.05	0.23	0.03	0.1	0.14	0.04	0.08	0.15	0.14	0.12	0.2	tr.	tr.
LOI	12.87	2.62	1.89	1.27	2.09	3.46	6.14	1.86	2.22	4.96	2.27	5.94	3.11	2.04	5.48	3.55	1.47	0.82
Total	99.76	98.09	99.84	100.01	99.82	99.56	99.82	99.03	99.93	99.17	99.17	99.34	99.55	99.31	99.26	99.71	99.31	99.4

grains. Permian sandstones mainly comprise rare metasiltstone and phyllite.

The proportion of the bulk heavy minerals is largest in the Late Carboniferous samples, followed by the Ordovician, Early Carboniferous and the Permian samples (Table 1). The Ordovician samples contain (in decreasing abundance) the ultrastable minerals zircon, tourmaline and rutile, and the less stable apatite within translucent heavy minerals (Fig. 7). The mostly rounded grains are about 20–60 μm, the olive-green tourmalines are sometimes larger (up to 100 μm) and most rutile grains are spherical. Early Carboniferous samples, although relatively low in the absolute content on translucent heavy minerals, display the largest variety of different heavy minerals. Beside rutile, zircon and tourmaline, garnet and apatite occur in most samples. Specifically, sample DM16a is characterized by its larger garnet content whereas other samples contain only minor proportions. In the Late Carboniferous sandstones, rutile dominates over tourmaline and zircon. The rutile grains display a rather altered appearance, possibly due to etching by intrastratal solution. Tourmaline represents the largest heavy mineral (up to 150 μm), besides olive-green variations some bluish-green grains occur. The Permian sandstone also contains mainly rutile, followed by tourmaline and zircon. The grain size of the few heavy minerals is generally in the range of 20–40 μm.

Whole-rock geochemistry

After their chemical classification of sandstones (Fig. 8a), the Late Ordovician and Devonian sandstones fall into the fields of greywacke and subarkose, the Early Carboniferous rocks plot into the greywacke and litharenite fields, the Late Carboniferous samples into the subarkose and arkose fields, and the Permian rocks in the litharenite, subarkose and arkose fields (Fig. 8a).

The Na_2O/K_2O-ratio of the Late Carboniferous rocks is low. The high abundance of detrital white mica in these samples displaces the element ratios of Na_2O/K_2O and SiO_2/Al_2O_3 (because of higher contents of Al_2O_3 and K_2O) into the arkose field, although no feldspar grains were detected in these sandstones (also indicated by the low sodium content). Furthermore, none of the samples plots in the quartz arenite range (<15% matrix and cement), in contrast to the detrital modal analysis of most Late Ordovician and Late Carboniferous samples. The spread of Late Carboniferous and Permian samples over several fields within the diagrams may be explained by variable compositions of matrix in addition to varying contents of detrital white mica.

A more suitable distinction, including shales, can be done by the SandClass diagram by Herron (1988), which uses the Fe_2O_3/K_2O-ratio for a better differentiation with respect to mineral stability. The Late Ordovician and Devonian rocks are classified as sublitharenites and shales, the Early Carboniferous Hochwipfel Group tur-

Table 4 Chemical composition of sandstones of the Carnic Alps. Trace elements obtained by ICP-AES respectively ICP-MS. *AG* Auernig Group; *BA* Bischofalm Quartzite;*GD* Gröden Formation; *GL* Grenzland Formation; *HB* Himmelberg Sandstone; *HW* Hochwipfel Group; *WD* Waidegg Formation; *ZF* Zollner Formation

ppm	DM1	DM20	DM22	DM4	DM5	DM15	DM10	DM11	DM14	DM12	DM2	DM21e	DM9	DM13	DM17	DM45	DM3	DM40
	GD	GL	GL	AG	AG	AG	WD	WD	HW	HB	GD	AG	HW	HW	HW	ZF	BA	HB
As											4.96	11.7	12.4	9.94	8.54	0.57	4.7	5.87
Ba	165	144	313	258	233	450	821	423	446	943	223	678	548	504	258	441	234	118
Be	3.23	0	0.52	0.2	0.88	0.96	1.16	0	0.97	2.29	1.29	2.52	0.74	1.06	1.37	1.41	0.16	0.28
Bi											0.27	0.28	0.18	0.1	0.11	0.37	0.07	0.04
Cd											tr.	0.31	0.19	0.4	0.33	0.25	3.52	0.22
Ce											61.8	90.22	60.31	56.51	48.03	77.63	37.78	52.25
Co	6.07	5.52	5.85	1.56	2.5	7.09	18.5	5.97	8.58	17	4.43	12.7	17.9	11	11.4	20	4.23	2.83
Cr	56.7	20.3	50.2	33.3	44.6	60	77.8	42.2	59.4	129	32.6	91.6	116	66.7	87.8	110	39.8	19.4
Cs											10.8	6.24	4.58	3.26	3.23	6.71	1.7	1.01
Cu	3.08	4.34	9.3	7.6	10	20	52	11.9	20.9	33.3	5	23	38.1	24.7	23.4	170	23.3	4.7
Dy											4.08	4.67	4.48	3.94	3.81	4.85	1.455	1.569
Er											2.31	2.63	2.71	2.04	2.05	2.64	1.086	0.899
Eu											0.92	1.53	1.3	1.16	0.98	1.74	0.415	0.386
Ga	23.7	6.68	14	8.64	12.2	18.5	19	13.3	18.3	33	16.5	27.9	21.6	14.2	15.2	21.9	6.62	5.28
Gd											4.13	5.48	4.89	4.35	3.93	5.65	1.958	1.933
Ge											1.54	1.71	1.41	1.29	1.29	1.78	0.93	0.76
Hf											7.6	6.59	5.2	5.16	5.08	6.02	7.66	10.1
Ho											0.86	1.04	1.06	0.84	0.87	1.02	0.382	0.313
In											0.04	0.06	0.04	0.03	0.04	0.06	0.02	0.01
La											35.72	45.78	29	28.45	24.51	36.46	20.66	24.43
Lu											0.38	0.39	0.43	0.32	0.36	0.34	0.194	0.169
Mo											0.18	0.43	0.82	0.75	1.22	0.3	3.25	0.14
Nb	13.5	5.47	9.61	6.42	17.5	20.4	16.8	16.9	13.5	19.5	11.75	18.68	11.79	8.78	9.44	24.44	7.28	6.37
Nd											29.80	38.31	27.59	24.1	22.34	36.3	12.48	19.08
Ni	23.3	13.2	19.6	7.42	5.96	23.4	49.5	29.1	26.4	54.7	16.6	36.3	53.7	32.2	41.6	50.6	21.7	6.28
Pb											12	27.7	14.3	11.4	11	7.05	8.96	10.9
Pr											8.01	9.58	6.9	6.35	5.66	8.77	3.65	5.11
Rb	229	44.5	97.2	55.7	70.4	123	106	73.2	83.5	173	140.5	159.3	111.5	74.59	62.97	121.5	43.35	27.88
Sb											1.3	1.08	1.37	1.16	0.82	0.54	1.65	0.14
Sm											6.09	7.2	5.88	5.12	4.75	7.1	2.45	2.7
Sn											3.63	4.67	2.42	1.68	1.72	2.89	1.02	0.66
Sr	156	34.6	56.5	44.4	54.7	64.4	77.5	89.8	86.4	73.9	63.2	179	116	72.6	106	67.5	23.6	39
Ta											1.18	1.67	0.99	0.77	0.838	1.8	0.673	0.536
Tb											0.67	0.84	0.78	0.68	0.63	0.87	0.279	0.256
Th	12.6	2.4	5.95	2.63	6.19	14.4	9.36	6.29	9.09	9.23	12.18	12.85	7.88	7.58	6.42	9.04	5.61	7.04
Tm											0.36	0.41	0.44	0.33	0.32	0.39	0.179	0.162
U											2.66	2.8	2.6	2.27	2.12	2.15	2.41	1.48
V	57.9	29	60.2	35.1	51.1	78.7	152	50.5	75.7	160	46.5	112	160	84.8	116	195	77.3	27.8
W											3.24	3	1.33	1.09	1.19	1.93	1.17	0.47
Y											24.1	28.7	27.7	23.2	22.9	27.3	11.5	8.86
Yb											2.55	2.58	2.74	2.12	2.24	2.24	1.143	1.11
Zn	47.3	22.2	43.2	15.4	38.1	84.2	92.2	46	52.5	101	36.5	75	93.3	53.3	66.9	87.9	44.2	17.7
Zr	140	72.9	131	66.9	145	426	229	181	259	135	278	261	202	203	192	230	320	405

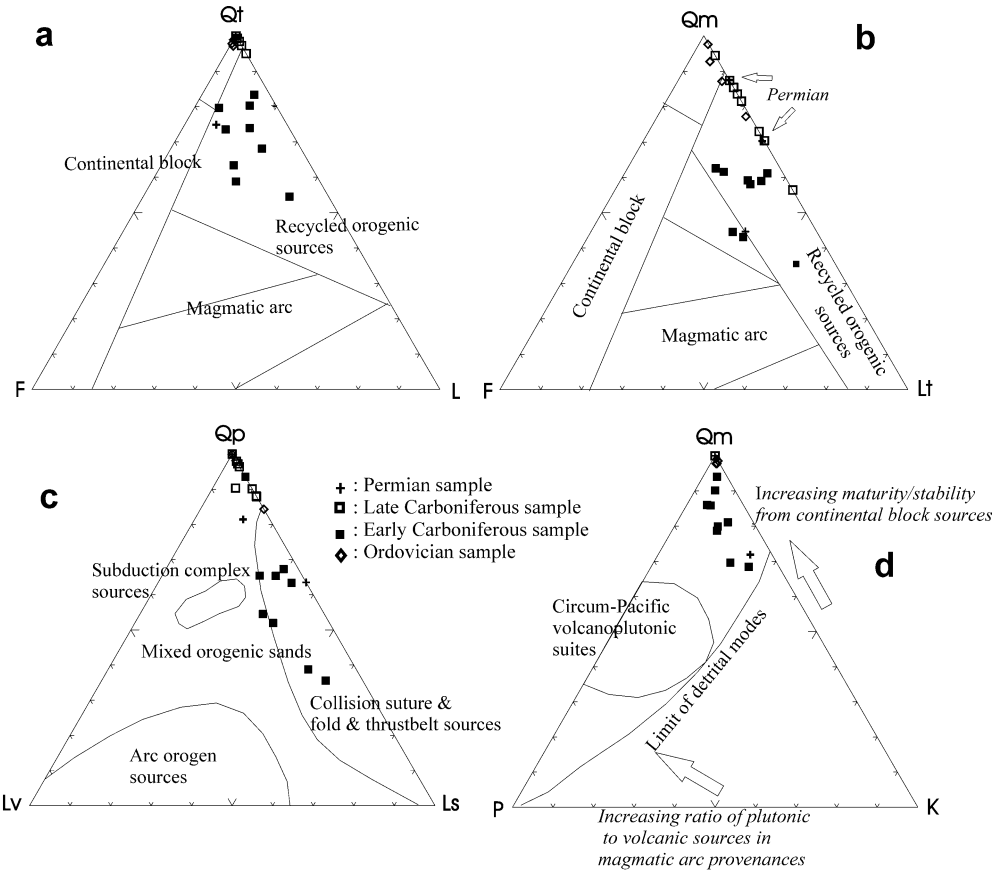

Fig. 6a–d QFL diagrams for provenance discrimination (after Dickinson et al. 1983; Dickinson 1985) and variation of mica contents in sandstones of various stratigraphic units. **a** Qt-F-L Qt = Qm+Qp; F = K+P; L = Ls+Lv+Lm; **b** Qm- F-Lt; Lt = Ls+Lv+Lm+Qp; **c** Qp-Lv-Ls; **d** Qm-P-K. For explanation of *abbreviations*, see text: Analytical methods and Table 1

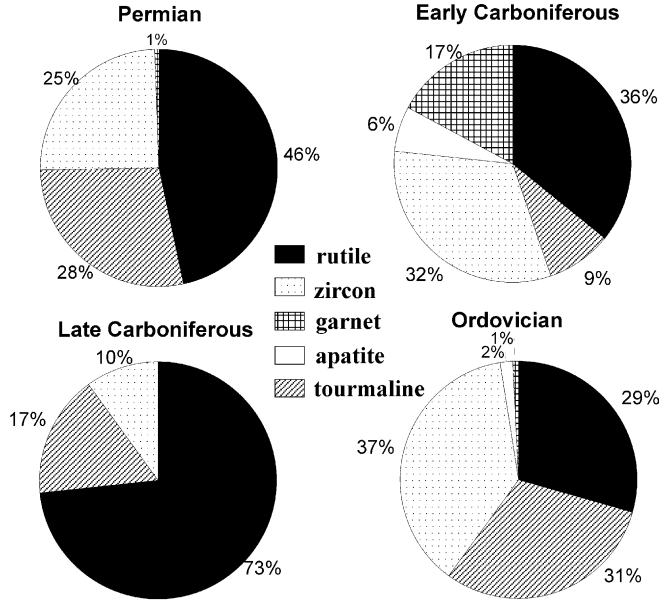

Fig. 7 Mean values (in grain percent) of heavy minerals of sandstones per stratigraphic unit in the Carnic Alps

biditic sandstones are displayed as wackes and shales, and the higher stratigraphic units are scattered over several fields between shale to subarkose (Fig. 8b), a pattern partly resulting from the variable amount of detrital white mica in these samples and the high clay content.

Plate-tectonic setting discriminations of ancient sedimentary basins are usually done using major and trace element bivariate plots. Although such graphs are not really significant for specific local plate tectonic settings, some correlations between tectonics and geochemical processes in sandstones, as well as the relationships and temporal and spatial variations of various lithostratigraphic units, can be evaluated.

The ratio of SiO_2 vs. (K_2O/Na_2O) provides a tectonic setting discriminator for sandstone–mudstone suites (Roser and Korsch 1986). In Fig. 9a, the investigated samples plot in the fields of passive (Late Ordovician, Late Carboniferous and Permian samples) and active continental margin settings (mainly Early Carboniferous samples). Samples DM12, DM45 and DM1 (one Late Ordovician, Devonian and Late Permian sample each) represent phyllosilicate-rich siltstones/fine-grained sandstones that show no reasonable patterns in most of the following whole-rock geochemistry plots; Fig. 9a).

After Bhatia (1983), four fields of principal tectonic settings can be distinguished using the correlation of ratios of K_2O/Na_2O, Al_2O_3/SiO_2 and $Al_2O_3/(CaO+Na_2O)$, plotted against TiO_2 or (Fe_2O_3+MgO), respectively. Those are passive margin (PM; recycled sedimentary and metamorphic source rocks), active continental margin (ACM; granites, gneisses, siliceous volcanics), continen-

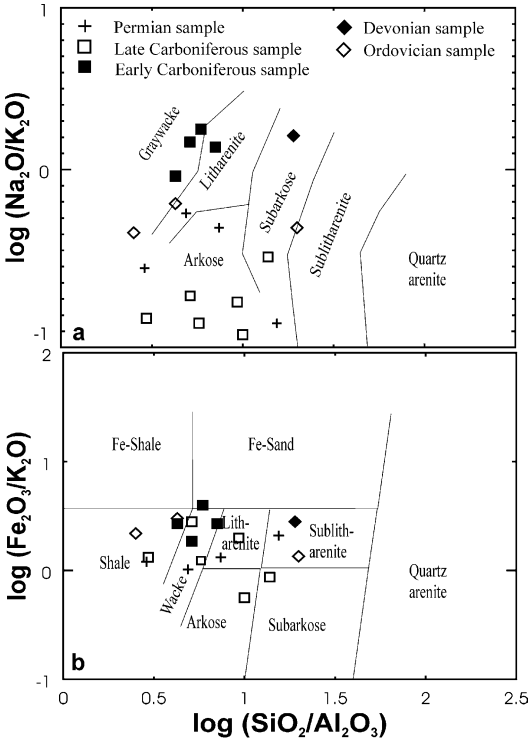

Fig. 8 a Classification diagram (after Pettijohn et al. 1972) discriminating siliciclastic sediments by their logarithmic ratios of SiO_2/Al_2O_3 and Na_2O/K_2O. **b** Classification diagram (after Herron 1988) discriminating siliciclastic sediments by their logarithmic ratios of SiO_2/Al_2O_3 and Fe_2O_3/K_2O

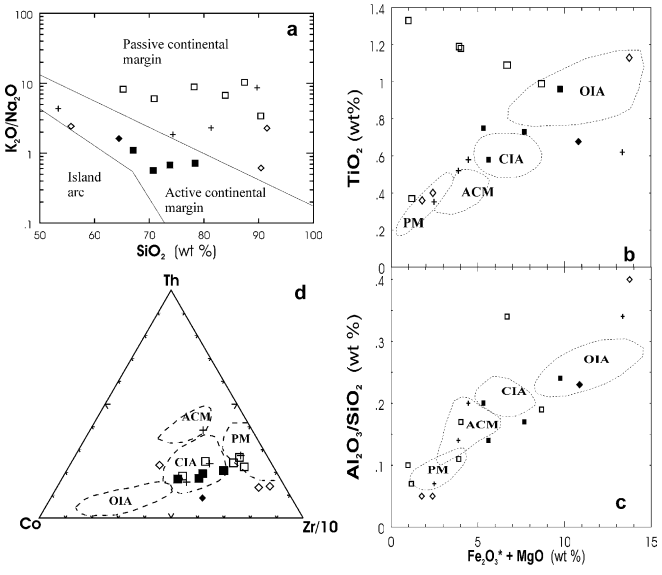

Fig. 9 Diagrams characterizing the tectonic setting by geochemical discrimination. **a** Discrimination diagram (after Roser and Korsch 1986) for differentiation of plate tectonic settings. **b** (Fe_2O_3*+MgO) vs. TiO_2. **c** (Fe_2O_3*+MgO) vs. Al_2O_3/SiO_2 discrimination diagrams (after Bhatia 1983). **d** Co–Th–Zr diagram for tectonic setting discrimination (after Bhatia and Crook 1986). *OIA* Oceanic island arc; *CIA* continental island arc; *ACM* active continental margin; *PM* passive margin. For description of plot symbols see Fig. 8

tal island arc (CIA; felsic volcanic source rocks) and oceanic island arc (OIA; calc-alkaline or tholeiitic rocks).

According to the TiO_2 vs. (Fe_2O_3+MgO) diagram (Fig. 9b), Early Carboniferous sandstones display oceanic and continental island arc settings. Late Carboniferous sandstones do not fit any of the tectonic setting fields because they show a negative correlation due to the high TiO_2 contents in these rocks, caused by the high amount of rutile (Fig. 7). Late Ordovician and Devonian samples plot in the fields of PM and OIA, the Permian samples in the PM and ACM fields. Due to its higher ferromagnesian contents, sample DM9 (Early Carboniferous) plots into the oceanic island arc field or even outside the entire field area. The OIA setting of one of the Late Ordovician sample (DM12) and the Devonian sample (DM45) is also explained by their high ferromagnesian contents, as they are matrix-rich siltstones (DM12 is a shaly siltstone/fine-grained sandstone with abundant biotite). One Late Permian sample (DM1) lies outside the proposed fields of tectonic settings due to its high amount of carbonate cement (dolomite?) and/or the clayey matrix.

According to the Al_2O_3/SiO_2 vs. (Fe_2O_3+MgO) diagram (Fig. 9c), the Late Ordovician and Devonian rocks fall into the fields of PM (and OIA, DM12), the Early Carboniferous sandstones lie near the fields of CIA, OIA and ACM (Fig. 9c). The Late Carboniferous samples plot in the PM, ACM and CIA fields and the Permian rocks in ACM and PM fields (except DM1).

In the diagrams of K_2O/Na_2O and $Al_2O_3/(CaO+Na_2O)$ vs. (Fe_2O_3+MgO) of Bhatia (1983; not shown), the widely scattered samples do not plot in the range of proposed fields of tectonic settings, and are mainly even outside the diagrams. Thus, these diagrams cannot be used for any interpretation. Several reasons may be responsible for this: (1) another kind of matrix (e.g. carbonate) as in the samples of Bhatia (1983); (2) secondary alteration of feldspar and lithic fragments (e.g. phyllosilicate formation), or (3) the high amount of detrital white mica and the low feldspar contents. Similar effects of no interpretable differentiation through e.g. varying elemental abundances of ultramafic source rock components in the sample matrix are mentioned in Toulkeridis et al. (1999).

The same four fields of tectonic setting as above can be discriminated by the use of the trace elements Th, Co and Zr (Bhatia and Crook 1986). In Fig. 9d, sandstones of the Early Carboniferous Hochwipfel Group plot into the CIA field, Late Carboniferous samples fall in the fields of PM and CIA, the Late Ordovician and Devonian rocks plot close to PM and CIA settings, and the Permian samples are assigned to CIA, ACM and PM settings (Fig. 9d). Some of the Late Ordovician, Devonian, Late Carboniferous and Permian samples plot into the ranges of continental island arc and active continental margin, which might partly be explained by the Co content, possibly concentrated in the clay fraction of these fine-grained rocks. As mentioned in McLennan et al. (1990),

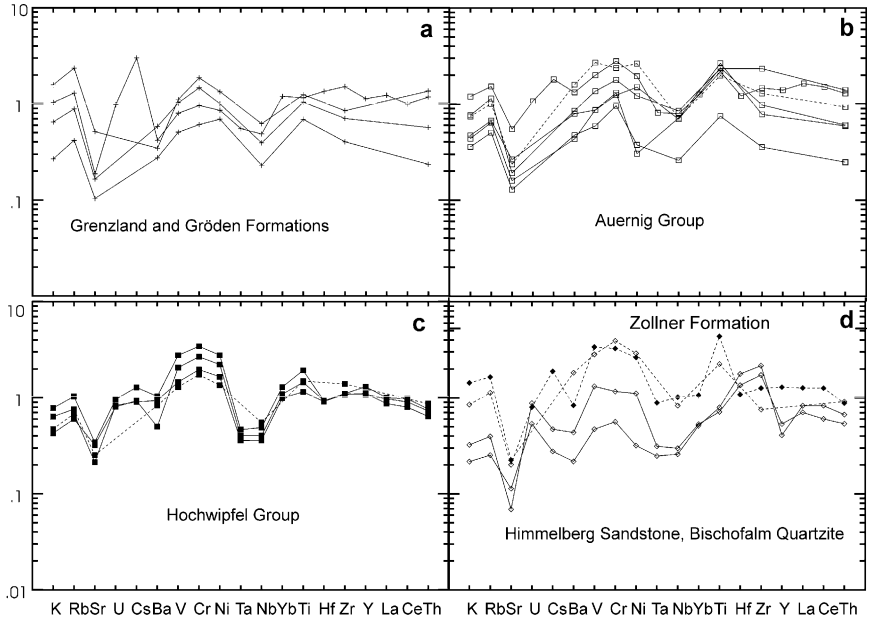

Fig. 10 Multi-element diagrams normalized to average upper continental crust composition (after Floyd et al. 1991). **a** Permian. **b** Late Carboniferous. **c** Early Carboniferous. **d** Ordovician and Devonian. Note that the higher proportion of Ti may rather be due to the mafic volcanic input than to recycled heavy minerals. Ti values correlate in a positive way with elements like V, Cr or Ni, indicating a contribution of Ti by mafic igneous rock fragments rather than by stable heavy minerals like rutile. Siltstones are shown by *dashed lines*

some elements (as, e.g., Cr, Ni, Co, Ba) are influenced by weathering and sedimentation (dissolution, transport, deposition, diagenesis) and thus can be enriched in the mud fraction by such processes.

Multi-element diagrams (Fig. 10) seem to be better indicators for the tectonic environment than bivariate plots, which are strongly influenced by contents of heavy minerals, mafic input and the degree of sorting. They can show heavy mineral and mafic volcanic input, too. High SiO_2 contents dilute most trace elements so that geochemical patterns can shift to lower values than unity, but still preserving relative enrichments and depletions within the pattern.

Inconsistent patterns are indicated by the Permian samples, where DM2 displays a very high portion of Cs (Fig. 10a). Two samples indicate rather high values of V–Cr–Ni, the peaks of Ti–Hf–Zr are rather low.

The Late Carboniferous sandstones also display in part positive V, Cr, Ni, Ti, Hf and Zr anomalies (Fig. 10b). The Nb and Ta values are partly close to the normalization values, which may indicate a relation to an oceanic intraplate environment. Thus, this group is mainly characterized as continental arc/active margin tectonic environment (and partly as a passive) setting. This is an unlikely conclusion in view of the evidence favouring the molasse nature of the formations of this age because generally molasse-type settings are geochemically indicated as a passive continental margin setting.

Samples from the Early Carboniferous Hochwipfel Group show the most homogeneous pattern. They are interpreted as a continental arc/active margin tectonic environment (CAAM). The positive V–Cr–Ni anomaly is relatively high and there are negative Nb–Ta and a slightly positive Ti–Hf–Zr anomalies (Fig. 10c). Higher mafic input and subduction-related influence is indicated by the first two anomalies, whereas the low positive Ti–Hf–Zr anomalies suggest a slight influence of mature sedimentary detritus (zircon, rutile) of a passive continental margin.

Using the normalization procedure proposed by Floyd et al. (1991), the Late Ordovician samples display positive Hf and Zr, but negative Ti and Y anomalies, indicating high zircon contents (Fig. 10d; and compare with Fig. 7). In two cases (silt-sized DM12, 45, the latter is Devonian) the V–Cr–Ni anomaly is very high. Nb–Ta abundances near the normalization value in these rocks suggest a contribution of oceanic intraplate material, but this may be influenced by the high phyllosilicate contents. In general, the Ordovician samples are interpreted as a passive continental margin-type setting.

The strongly negative Sr-anomaly, which is typical for old recycled environments/passive continental margin settings, is common in all of the samples. This low Sr ratio relates to low CaO contents, probably due to dissolution of plagioclase feldspar.

Rare earth elements of clastic sedimentary rocks are generally very sensitive tools for provenance studies because of their relative immobility during alteration by weathering, diagenesis and sedimentary processes (e.g. McLennan 1989). Some fractionation and mobilization of the REE, however, may occur by source rock weathering (e.g. Nesbitt 1979; Banfield and Eggleton 1989; Nesbitt et al. 1990; Morey and Setterholm 1997; Zhang et al. 1998).

REEs were analysed from every investigated stratigraphic unit (Fig. 11), mostly from the Early Carboniferous Hochwipfel Group flysch (DM9, 13, 17). The latter displays lower LREE contents than samples from other stratigraphic units (Table 5). They show lower Eu depletion (0.69–0.75) than expected from immature sediments, such as greywacke with their large proportion of unstable mafic components. Sample DM45 from the Devonian Zollner Formation shows a similar pattern. By

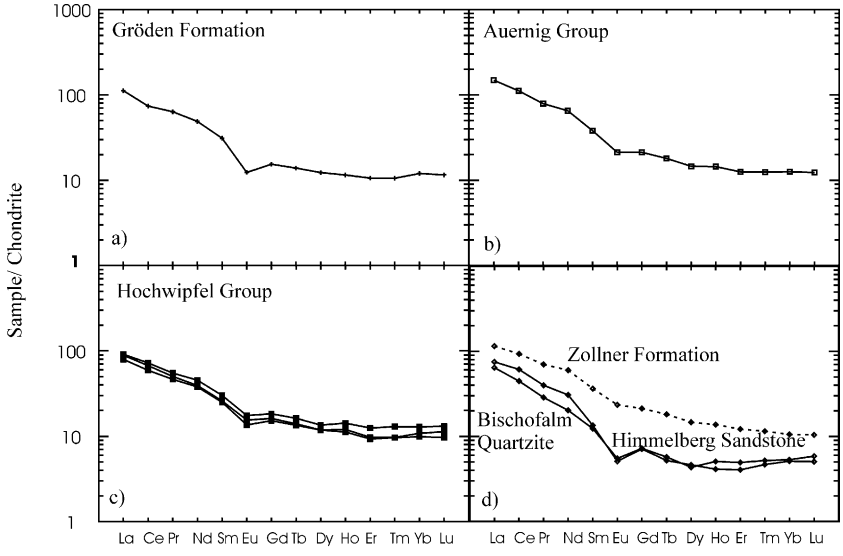

Fig. 11 Chondrite-normalized REE patterns. **a** Late Permian; **b** Late Carboniferous; **c** Early Carboniferous; **d** Late Ordovician and Devonian. Normalization values after Evensen et al. (1978, cited in Taylor and McLennan 1985)

contrast, Late Ordovician sandstones (DM3, 40) demonstrate a high negative Eu anomaly (0.52–0.58) and an enrichment of the LREE. A similar pattern is indicated by the Late Permian sample (DM2). The Late Carboniferous sample (DM21e) shows a similar feature as the Hochwipfel Group. The generally similar pattern of all samples shows a typical upper crustal composition and may be interpreted as indicators for a rather mature continental source (Fig. 11).

According to Bhatia (1985), several REE characteristics (La, Ce, ΣREE, La/Yb, La_N/Yb_N, ΣLREE/ΣHREE, Eu/Eu*; Table 5) are useful to discriminate the tectonic setting of sedimentary basins. In this study, we used the Eu/Eu* equation after Taylor and McLennan (1985), but the values calculated using Bhatia's equation (Bhatia 1985) are nearly identical (deviation of the ratio of only –0.02 and –0.03) and make no difference in the interpretation. Late Ordovician and Devonian samples (DM3, 40; DM45) do not show suitable correlations, and indicate different sources, the Devonian sample resembling rather to Early Carboniferous patterns. Various tectonic settings as continental island arc (suggested by La, Ce, ΣREE), passive margin (as indicated by Eu/Eu*, La/Yb, La_N/Yb_N) and Andean-type continental margin (due to La, Ce, ΣREE, ΣLREE/ΣHREE abundances of the Devonian sample) are indicated. The Carboniferous samples (DM9, 13, 17; DM21e) display a better and fairly homogeneous correlation with Bhatia's discrimination scheme (Table 5). Thus, sandstones of the Hochwipfel Group are depicted as continental island arc setting through all discrimination values. A passive-margin setting is shown for the post-orogenic Late Carboniferous Auernig Group; only the ΣLREE/ΣHREE and Eu/Eu* ratios suggest a continental island arc setting. By contrast, the Permian sample (DM2), with the exception of the Eu/Eu* ratio, which indicates a passive margin setting, a continental island arc/Andean-type continental margin setting is indicated (ΣLREE/ΣHREE ratio, La, Ce, ΣREE, La/Yb, $(La/Yb)_N$).

Composition of detrital white mica

The results of electron microprobe analysis (Table 6) were plotted in ternary diagrams (Fig. 12) with the compositional mol-percentage of muscovite, paragonite and celadonite. The chemical composition of white mica should reflect the nature of magmatic and metamorphic source rock (Speer 1984; Spear 1993). Mica compositions close to the muscovite corner indicate provenance from granites and regionally metamorphosed rocks. The more phengitic populations point to high-pressure metamorphic source rocks from deeper orogenic levels exposed by exhumation (as the phengite content is largely formed by high pressure); high paragonite compositions indicate low- to medium-grade metamorphic source rocks.

Mica composition varies through time, and analyses from thin sections and from magnetically separated concentrates yield, as expected, different results (Fig. 12). The Ordovician multigrain concentrate shows a relatively narrow cluster near the muscovite corner. Both Early Carboniferous multigrain concentrates display a slightly scattered pattern with a main spread along the muscovite–paragonite axis (Fig. 12). The Early Carboniferous micas in thin sections display a spread along the muscovite to celadonite axis.

The micas in the Late Carboniferous multigrain concentrate (DM4) have, apparently, two distinct mica populations and significantly higher paragonitic contents than the chemically more diverse Early Carboniferous ones (Fig. 12). Micas in thin sections spread mainly along the muscovite–phengite axis.

The micas from the multigrain concentrate of the Early Permian sample (DM22) plot to higher sodium contents (paragonitic composition), whereas the phengitic component is generally not more than 20% (Fig. 12). The micas in the thin section from the Late Permian sample also cluster near the muscovite corner, with a slight spread to the phengitic side.

Table 5 REE characteristics for tectonic setting discrimination of sedimentary basins (after Bhatia 1985). *ATCM* Andean-type continental margin; *CIA* continental island arc; *PM* passive continental margin. Italic numbers are data from Bhatia (1985). Sample symbols are explained in Fig. 5

Provenance type		La	Ce	ΣREE	La/Yb	La_N/Yb_N	ΣLREE/ΣHREE	Eu/Eu*	Tectonic setting
Undissected magmatic arc		*8±2*	*19±4*	*58±10*	*4.2±1.3*	*2.8±0.9*	*3.8±0.9*	*1.04±0.11*	Oceanic island arc
Dissected magmatic arc		*27± 5*	*59±8*	*146±20*	*11±4*	*7.5±2.5*	*7.7±1.7*	*0.79±0.13*	Continental island arc
Uplifted basement		*37*	*78*	*186*	*12.5*	*8.5*	*9.1*	*0.60*	Andean-type continental margin
Craton interior tectonic highlands		*39*	*85*	*210*	*15.9*	*10.8*	*8.5*	*0.56*	Passive continental margin
DM2	GD (plus)	35.72	61.80	156.02	14.01	9.47	9.69	0.56	ATCM, CIA, PM
DM21e	AG (empty square)	45.78	90.22	208.33	17.74	11.99	11.08	0.74	PM, CIA
DM9	HW (filled square)	29.00	60.31	146.34	10.58	7.15	7.78	0.74	CIA
DM13	HW (filled suare)	28.45	56.51	134.50	13.42	9.07	8.63	0.75	CIA
DM17	HW (filled square)	24.51	48.03	118.82	10.94	7.39	7.78	0.69	CIA
DM45	ZF (diamond)	36.46	77.63	183.53	16.28	11.00	9.63	0.84	ATCM, PM
DM3	BA (diamond)	20.66	37.78	83.323	18.08	12.21	12.22	0.58	CIA, PM
DM40	HB (diamond)	24.43	52.25	109.65	22.01	14.87	17.03	0.52	CIA, PM

Barium and titanium are supposed to be provenance-significant elements in white mica (Speer 1984). The element barium is more abundant in white micas from granitic/pegmatitic rocks; titanium is more abundant in micas from intermediate plutonic rocks (Speer 1984, with references). Thus the variation of these elements may indicate different provenances for detrital white micas (Fig. 13). A higher abundance of iron (together with magnesium in phengite) in white micas indicates a metamorphic origin. Generally, igneous muscovites have more Ti, Al, Na and less Mg, Si and Fe (Speer 1984). Ba and Ti are plotted against Na/(Na+K), and Fe/(Fe+Mg) (Fig. 13; Ti plots are not shown).

Ordovician micas (DM3, 12), which were only measured as multigrain concentrates, are characterized by a Ba content in the range of ca. 0.0–0.8 wt% and a low variation along the Na/(Na+K) axis. This pattern is also shown by the other groups, with the exception of the Early Carboniferous micas, which scatter over a broader compositional range (Fig. 13). The Late Carboniferous micas generally show the lowest Ba content (<0.4 wt%) with the largest spread in the Na/(Na+K) ratio within the thin sections. The multigrain concentrates demonstrate the same variation regarding the Ba contents, but in the Na/(Na+K) contents a narrower cluster occurs when compared with the other specimen groups. Two clusters in the Permian group are represented by two distinct samples (DM2, 22). The micas from the Early Permian sample (DM22) include the highest Na/(Na+K) contents (Fig. 13).

Similar patterns are shown by Ba vs. Fe/(Fe+Mg) plots. The Early Carboniferous micas exhibit a more scattered pattern than the others. The Fe/(Fe+Mg) ratio of the Permian sample, however, shows no separate cluster.

In summary, the Ba contents lie in the range of 0.0–0.8 wt%. Late Carboniferous samples display low values (<0.4 wt%). The wide Na/(Na+K) and narrow Fe/(Fe+Mg) variations of the Late Permian sample is also noticeable. All the other samples demonstrate a larger spread in the element ratios than in the barium contents.

Titanium shows the same picture when plotted against the Na/(Na+K) and Fe/(Fe+Mg) ratios (plots not shown). Remarkable, is the larger spread of the Early Carboniferous Ti contents compared with the other micas, even if compared with the Ba relations.

Composition of detrital feldspar

Additional to detrital white mica, some feldspars were analysed in thin sections from the Early Carboniferous Hochwipfel Group (DM9, 13, 17) and the Permian Gröden Formation (DM2; Table 7). Feldspar is scarce in other samples. Very high sodium, moderate calcium and low potassium contents suggest albite and predominant oligoclase compositions (Fig. 14). The Permian feldspars comprise lower potassium contents than those of the Early Carboniferous samples. The high albite proportion may be an artifact of their better visibility in the back-scattered electron image than that of the potassium feldspars: the latter are more difficult to distinguish from quartz grains. The high albite, i.e. oligoclase contents may also reflect, in part, the high albite, i.e. oligoclase, stability and, in part, post-depositional albitization. However, the presence of oligoclase with minor K_2O content suggests derivation from igneous, acidic to intermediate, rocks.

Discussion

The Late Ordovician to Permian stratigraphic sequence was investigated using only a small amount of samples. Therefore, we can only demonstrate the general variability and trends in the geodynamic setting of these lithostratigraphic sequences. However, results from previous studies using the modal analysis approach (Fontana and Venturini 1982; Hinderer 1992; Krainer 1992; Poscheschnik 1993) are largely in agreement with our

Table 6 Representative electron microprobe analyses (wt%) of detrital white micas from sandstones of the Carnic Alps

Label	SiO_2	Al_2O_3	MgO	Na_2O	TiO_2	CaO	K_2O	FeO	MnO	Cl	BaO	Cr_2O_3	Total
Thin sections: GD (DM2), AG (DM5, 21e), HW (DM9, 13, 17)													
DM2/5	45.80	34.90	0.82	0.31	0.41	0.06	9.76	1.33	0.03	0.04	0.05	0.01	93.43
DM2/18	45.69	35.20	0.71	0.39	0.79	0.00	10.00	1.30	0.02	0.01	0.11	0.01	94.20
DM5/2	46.82	33.44	1.05	1.11	0.31	0.02	8.81	2.34	0.01	0.00	0.19	0.04	94.08
DM5/8	46.90	33.48	1.12	0.74	0.31	0.00	9.28	1.85	0.00	0.00	0.20	0.03	93.87
DM5/10	49.15	27.73	2.53	0.13	0.27	0.06	10.24	3.47	0.05	0.01	0.29	0.01	93.93
DM5/22	49.98	26.19	2.68	0.15	0.46	0.01	10.24	3.65	0.04	0.00	0.27	0.06	93.68
DM21e/7	48.06	29.73	2.15	0.64	0.34	0.22	9.85	2.92	0.00	0.00	0.27	0.02	94.16
DM21e/8	49.61	27.50	2.66	0.29	0.29	0.12	9.86	3.11	0.02	0.01	0.28	0.02	93.71
DM21e/12	49.38	27.60	2.89	0.35	0.35	0.16	9.89	2.98	0.01	0.01	0.27	0.02	93.86
DM9/1	48.88	28.05	2.81	0.16	0.26	0.04	10.27	3.23	0.04	0.01	0.45	0.01	94.15
DM9/2	47.54	32.86	1.66	0.73	0.67	0.02	9.25	1.14	0.01	0.01	0.27	0.03	94.12
DM9/17	48.44	29.83	2.36	0.66	0.66	0.04	9.51	2.63	0.00	0.00	0.32	0.07	94.52
DM9/24	48.36	29.01	3.16	0.30	0.59	0.01	10.38	1.71	0.08	0.00	0.74	0.04	94.32
DM13/3	48.91	29.17	2.64	0.44	0.41	0.01	9.36	2.68	0.00	0.00	0.34	0.00	93.95
DM13/9	48.98	29.40	2.85	0.24	0.57	0.03	10.05	1.93	0.04	0.00	0.53	0.01	94.54
DM13/21	47.35	31.06	2.68	0.11	0.04	0.05	9.40	3.77	0.01	0.00	0.06	0.02	94.41
DM13/28	47.15	33.44	1.08	0.72	0.27	0.02	9.29	1.98	0.03	0.01	0.23	0.06	94.22
DM17/1	48.87	31.76	1.77	0.61	0.62	0.07	9.19	1.28	0.01	0.00	0.31	0.06	94.54
DM17/12	46.79	33.01	1.40	0.34	0.87	0.12	10.63	1.17	0.03	0.02	0.29	0.05	94.63
DM17/16	47.96	31.65	1.88	0.41	0.64	0.34	9.76	1.67	0.02	0.02	0.50	0.04	94.81
DM17/23	48.00	26.56	2.37	0.17	0.21	0.29	10.75	5.57	0.05	0.01	0.24	0.01	94.21
Multigrain concentrates: GD (DM2), GL (DM22), AG (DM4), HW (DM9, 14), BA (DM3), HB (DM12)													
DM2/3	46.00	35.30	0.73	0.49	0.72	0.00	10.20	1.03	0.00	0.00	0.25	0.00	94.79
DM2/4	46.80	34.90	1.03	1.36	0.57	0.00	8.60	1.20	0.00	0.00	0.37	0.00	94.86
DM2/8	45.30	35.10	0.58	0.45	0.54	0.00	10.40	1.17	0.00	0.00	0.11	0.00	93.68
DM2/9	45.90	34.40	0.88	0.31	0.85	0.00	10.70	0.95	0.00	0.00	0.14	0.00	94.10
DM22/1	46.50	36.48	0.49	2.30	0.24	0.00	7.47	0.83	0.00	0.00	0.69	0.00	95.01
DM22/3	47.07	34.61	1.00	1.17	0.52	0.00	9.28	0.76	0.00	0.25	0.50	0.00	94.94
DM22/4	46.29	36.60	0.53	2.23	0.30	0.00	7.69	0.82	0.00	0.00	0.16	0.00	94.71
DM22/10	45.91	35.53	0.57	1.57	0.27	0.00	8.72	0.82	0.00	0.03	0.19	0.00	93.43
DM4/1	45.70	35.80	0.55	0.93	0.16	0.00	9.50	1.25	0.00	0.00	0.24	0.00	94.18
DM4/3	46.40	35.50	0.72	1.47	0.27	0.00	8.50	1.12	0.00	0.00	0.28	0.00	94.29
DM4/7	48.20	32.10	1.51	1.08	0.32	0.00	8.70	1.94	0.00	0.00	0.24	0.00	94.01
DM4/15	45.50	35.60	0.52	1.38	0.34	0.00	8.90	0.78	0.00	0.00	0.26	0.00	93.18
DM9/3	46.20	35.80	0.75	2.12	0.61	0.00	7.70	0.76	0.00	0.00	0.14	0.00	94.15
DM9/4	45.90	35.70	0.75	1.15	0.57	0.00	9.20	0.73	0.00	0.00	0.73	0.00	94.69
DM9/6	45.50	33.40	1.52	0.46	1.59	0.00	10.40	0.57	0.06	0.00	0.48	0.00	94.04
DM9/7	46.20	34.30	1.16	0.77	0.95	0.00	9.80	0.61	0.00	0.00	0.53	0.00	94.29
DM14/1	46.99	32.44	1.85	0.34	0.26	0.00	10.22	1.32	0.00	0.00	0.00	0.00	93.42
DM14/2	46.99	33.97	1.19	1.13	1.14	0.00	9.38	1.36	0.00	0.00	0.18	0.00	95.33
DM14/10	45.28	32.43	0.91	0.51	0.75	0.00	10.19	4.01	0.00	0.00	0.45	0.00	94.54
DM14/14	46.47	33.13	1.14	0.33	0.39	0.00	10.42	1.92	0.00	0.00	0.16	0.00	93.96
DM3/3	47.11	32.65	1.35	1.04	0.23	0.00	9.31	2.07	0.00	0.00	0.17	0.00	93.92
DM3/8	46.60	32.08	1.55	0.67	0.56	0.00	9.45	1.70	0.00	0.00	0.56	0.00	93.17
DM3/13	47.16	31.14	1.91	0.98	0.69	0.00	9.13	2.12	0.00	0.00	0.36	0.00	93.49
DM3/14	44.37	28.36	1.96	0.57	0.74	0.00	8.35	4.97	0.00	0.00	4.51	0.00	93.82
DM12/1	45.60	34.00	1.04	0.75	0.72	0.00	9.60	1.12	0.00	0.00	0.32	0.00	93.10
DM12/8	45.60	33.40	1.17	0.73	0.85	0.00	9.50	1.42	0.00	0.00	0.83	0.00	93.59
DM12/10	45.70	33.90	1.15	0.44	0.36	0.00	10.50	1.39	0.00	0.00	0.11	0.00	93.55
DM12/14	45.30	35.40	0.56	0.81	0.84	0.00	9.90	1.04	0.00	0.00	0.27	0.00	94.18

results and underline the significance of our mixed petrographic/geochemical approach.

Our new data from various sandstones of the Carnic Alps have significance both for the Palaeozoic evolution of the Carnic Alps and for the use of petrographical and geochemical analysis of sandstones. First we discuss the new data in comparison with existing geodynamic models of the Carnic Alps (Fig. 15), which are based on data mentioned before (for data compilation, see Schönlaub and Histon 2000; Neubauer and Handler 2000; Läufer et al. 2001). We do not discuss in detail the Devonian evolution as our data base is too small, although the indication of a subduction-related environment is noticeable and should be clarified in a further study. Specifically geochemical indicators plead for an enrichment of a mafic volcanic input. However, because of its low sedimentation rate, less than 200 m for Silurian and Devonian, a secondary enrichment of mafic volcanic components cannot be excluded. Finally, we argue for a more complex approach using modal and geochemical indicators for provenance studies.

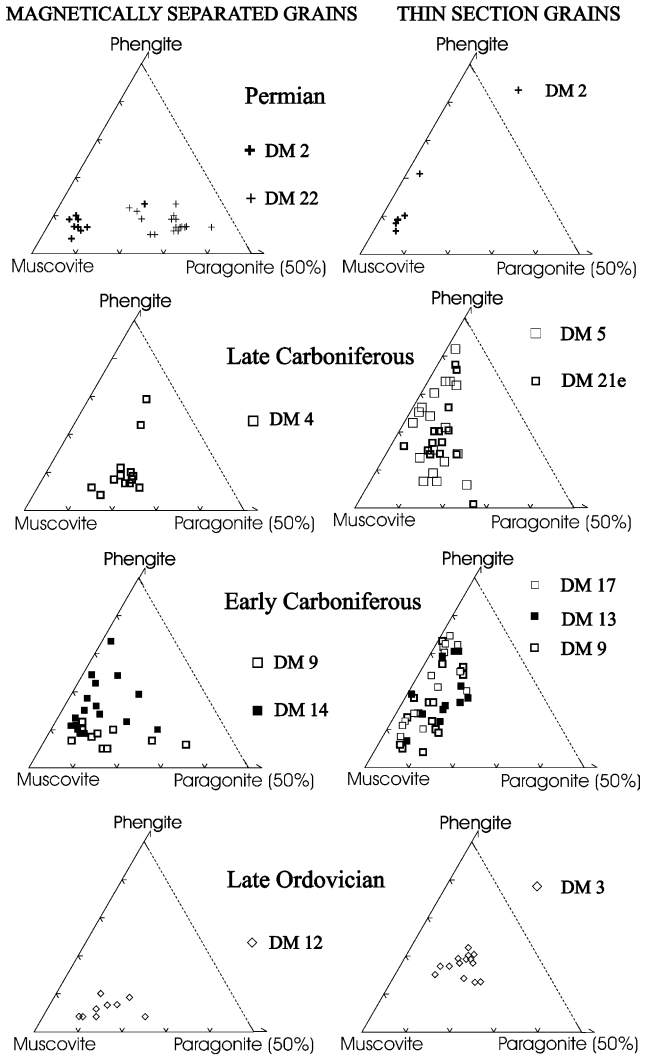

Fig. 12 Ternary plots showing the chemical variation of detrital white mica determined by electron microprobe. Note that samples plot in distinct clusters in different age levels. For example, the Ordovician multigrain concentrate show a relatively narrow cluster near the muscovite corner with a small spread to the paragonite corner, whereas in the thin section the mica suggest more phengitic and paragonitic compositions

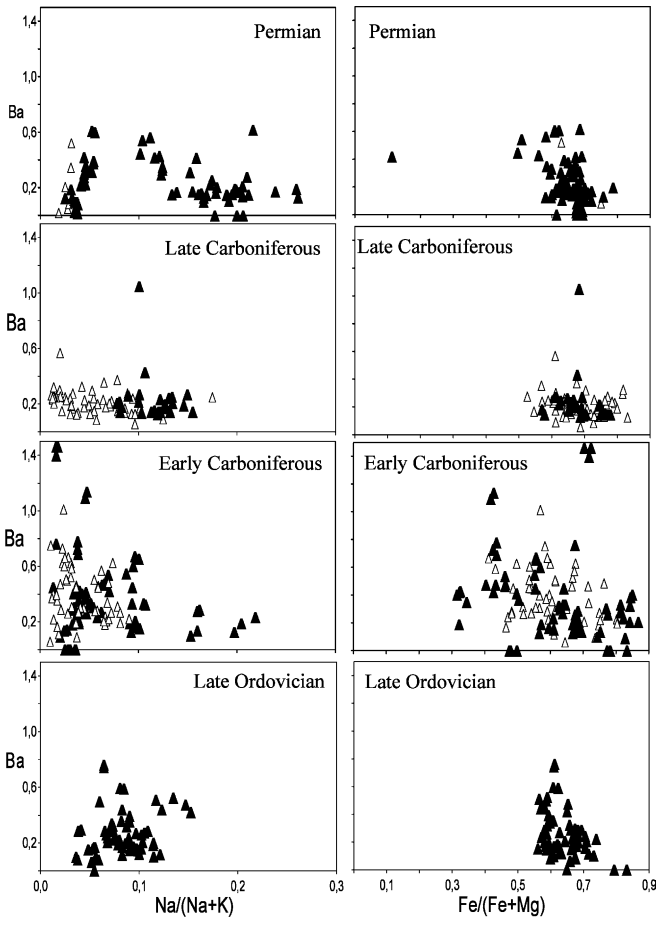

Fig. 13 Ba vs. Na/(Na+K) and Ba vs. Fe/(Fe+Mg) diagrams indicating the compositional variations of detrital white micas in different lithostratigraphic units: *open triangles* white micas measured in thin section; *filled triangles* multigrain concentrates

Late Ordovician

According to the QFL and Q_mFL_t diagrams, Late Ordovician sandstones are derived from the continental block/craton interior or a recycled orogenic source and can be interpreted as passive continental margin sediments, in accordance with results from previous modal analyses (Poscheschnik 1993). These samples are nearly exclusively composed of quartz grains, which are subangular to well rounded. The occurrence of the ultrastable heavy minerals zircon, tourmaline and rutile points to multicycled or strongly reworked material, typical for shallow marine and coastal environments in accordance with observations on facies evolution by Poscheschnik (1993).

Geochemically, the Late Ordovician samples mainly reflect a passive continental margin setting, too. Some results suggest an island arc setting, which is also explained by the fine-grained, matrix-rich composition of these samples (DM12). Maybe, due to their higher concentration of ferromagnesian elements (e.g. Al, Fe, Co, Mg, Ti) in the clay minerals and the lower relative SiO_2 contents, these shaly siltstones do not plot into the passive continental margin field of the Bhatia diagrams. This may reflect the input from mafic and acidic volcanic sources, which also comprise underlying stratigraphic units (e.g. Hinderer 1992).

The micas from Ordovician samples with their muscovitic and paragonitic compositions and the Ba and Ti values are interpreted as grains derived from low- to medium-grade metamorphic source rocks of a Cadomian orogenic block (Dallmeyer and Neubauer 1994). A rather homogeneous source area is indicated by the relatively narrow clustering of the data.

Based on volcanic successions and overlying transgressive marine sequences, a back-arc environment is postulated for the Late Ordovician by previous authors

Table 7 Chemical composition (wt%) of feldspars of sandstones from the Carnic Alps. *DM2* Gröden/Val Gardena Formation; *DM9* 13, 17: Hochwipfel Group

Label	SiO_2	Al_2O_3	MgO	Na_2O	TiO_2	CaO	K_2O	FeO	MnO	Cl	BaO	Cr_2O_3	Total
DM2/26	64.77	22.78	0.01	9.57	0.00	3.25	0.11	0.00	0.00	0.01	0.00	0.02	100.48
DM2/27	65.63	21.73	0.00	9.84	0.01	2.56	0.30	0.06	0.00	0.00	0.09	0.00	100.12
DM2/27	66.19	21.40	0.00	9.76	0.00	2.04	0.24	0.07	0.01	0.01	0.13	0.04	99.83
DM2/30	65.39	21.86	0.00	9.50	0.04	2.67	0.30	0.08	0.02	0.01	0.05	0.00	99.80
DM9/37	67.90	19.74	0.00	10.96	0.00	0.52	0.07	0.06	0.01	0.00	0.00	0.03	99.26
DM9/43	69.01	19.93	0.02	11.37	0.02	0.24	0.05	0.04	0.02	0.01	0.02	0.02	100.64
DM9/45	67.74	19.56	0.01	11.24	0.01	0.28	0.05	0.06	0.00	0.00	0.00	0.02	98.93
DM13/2	68.78	19.76	0.00	11.16	0.00	0.09	0.08	0.06	0.00	0.00	0.04	0.01	99.92
DM13/16	66.32	21.58	0.02	9.72	0.01	1.07	0.87	0.19	0.02	0.01	0.07	0.00	99.75
DM13/29	65.13	21.89	0.00	9.63	0.00	2.75	0.24	0.08	0.00	0.00	0.01	0.02	99.71
DM13/31	62.66	23.47	0.01	8.44	0.02	4.70	0.27	0.16	0.02	0.00	0.02	0.00	99.70
DM17/5	66.39	21.14	0.04	10.35	0.01	1.99	0.03	0.01	0.01	0.01	0.01	0.00	99.94
DM17/7	67.61	20.54	0.02	10.47	0.00	1.07	0.24	0.02	0.00	0.01	0.00	0.00	99.92
DM17/34	69.23	19.41	0.02	10.54	0.04	0.48	0.08	0.11	0.00	0.01	0.01	0.00	99.85

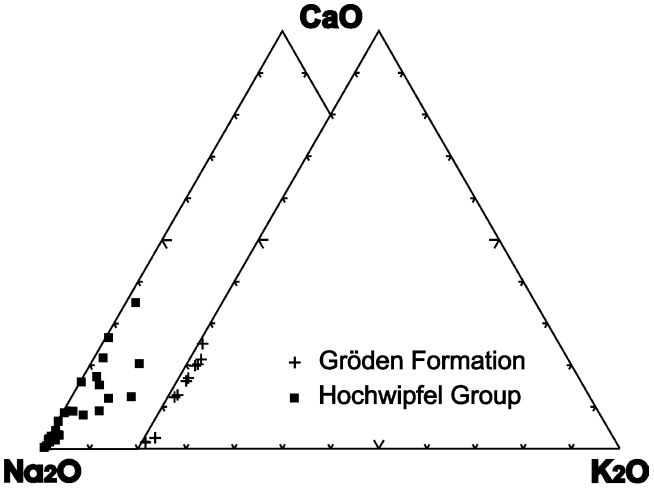

Fig. 14 Na_2O–CaO–K_2O diagram showing the albite and oligoclase compositions of feldspar grains of the Hochwipfel Group and Gröden Formation

(e.g. Hinderer 1992). This is in line with large-scale reconstructions postulating an Ordovician break-off of Alpine terranes blocks from Gondwana (e.g. Stampfli et al. 2002).

Early Carboniferous

Early Carboniferous samples are displayed as quartz-rich litharenites or greywackes. QFL plots suggest their derivation from a recycled orogenic source (mainly quartzose recycled). In a $Q_pL_vL_s$ diagram, these greywackes are characterized as material derived from collision-suture and fold-and-thrust-belt sources, with some tendency to subduction complex sources. The rather mature composition from continental block sources is indicated in the Q_mPK diagram (Fig. 6d). The mixed compositions indicate both a volcanic and orogenic source, the latter eroding a metamorphic orogenic wedge.

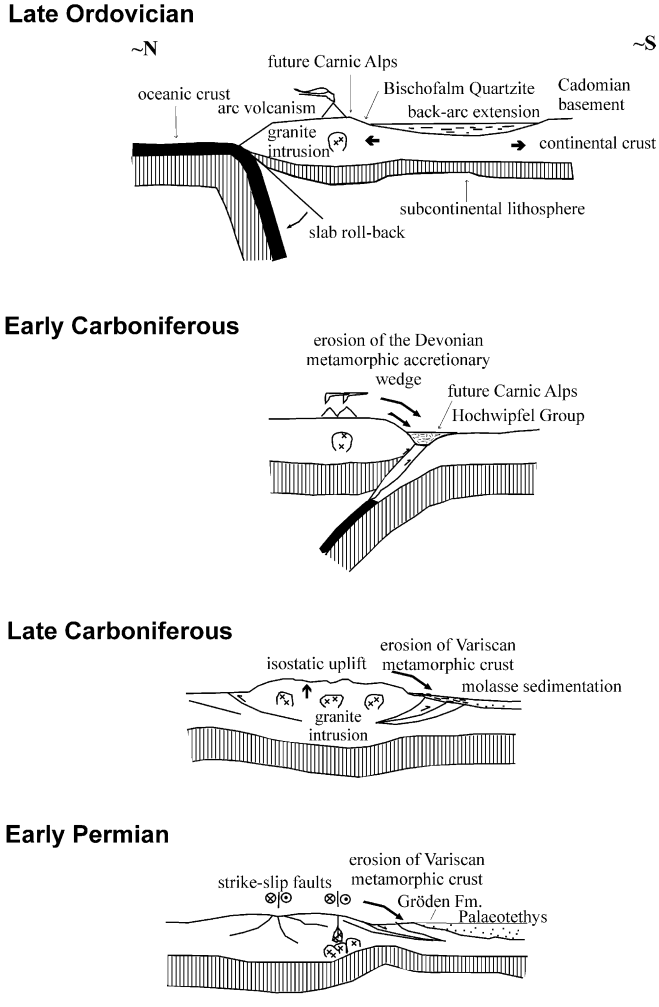

Fig. 15 Ordovician to Permian tectonic evolution of the Carnic Alps. For arguments and explanation, see text. Note uncertain orientation of suggested subduction zone during Late Ordovician. Assuming subsequent separation of a terrane comprising Carnic Alps from Gondwana, ca. southward subduction would be the most reasonable solution

The latter is confirmed by Devonian ages of detrital white mica (Mader et al. 2000).

From all groups analysed, only the Early Carboniferous Hochwipfel Group represents a homogeneous geochemical pattern. The sandstones of the Early Carboniferous Hochwipfel Group, mainly classified as greywackes, geochemically represent continental island arc and active continental margin settings (Fig. 15). It is known that the Variscan orogeny resulted in a final collision of two continents after the previous accretion of several Gondwana-derived terranes to the northern European continent (e.g. Frisch and Neubauer 1989; Neubauer and Handler 2000; Stampfli et al. 2002). Subduction occurred to the north-west below the active continental margin of the European continent, as indicated e.g. by Early Carboniferous granite intrusions in the Alps and the Moldanubian units, which were part of the northern terranes (e.g. Finger and Steyrer 1990). According to the position of the data points in the CIA and ACM fields, we interpret deposition in a fore-arc basin formed in front of an eroding continental island arc system during the Early to Late Carboniferous collision of two continental plates (e.g. Neubauer and Handler 2000; Läufer et al. 2001, and references therein). This confirms the existing interpretation of these syn-orogenic greywackes as turbiditic deposits (flysch; e.g. Spalletta et al. 1980; Spalletta and Venturini 1988; Läufer et al. 1993, 2001), which accumulated in a trench near a continental island arc or active continental margin. Compression in the Early Carboniferous is also reflected by structural data. The Palaeozoic Carnic Alps are a highly shortened, WNW–ESE-oriented, south-verging fold-and-thrust belt which was deformed in the Late Namurian/Westphalian (Venturini et al. 1990a; Schönlaub and Heinisch 1993; Schönlaub and Histon 2000; Läufer et al. 2001).

The micas of the Early Carboniferous samples display a fairly diverse chemical composition, both within each sample and between the individual samples. Hence, diverse source regions can be assumed for these samples. The relatively high phengitic components (up to 70 rel.%) of some of the micas point to a possible high-grade metamorphic source region together with paragonitic micas from rocks of low- to medium-grade metamorphic origin. The barium and titanium contents of the micas may be, according to Speer (1984), interpreted as minerals of originally plutonic rocks (granites).

Thus, the phengitic mica composition and the Devonian $^{40}Ar/^{39}Ar$ ages of white mica (Mader et al. 2000) of the Early Carboniferous Hochwipfel Group are interpreted to represent magmatic and metamorphic sources of an uplifted, exhumed and denuding Devonian accretionary wedge, which formed prior to Variscan continent–continent collision.

Late Carboniferous

Although molasse characteristics are obvious from facies analysis (e.g. Venturini 1990a, 1990b; Krainer 1992), sandstones of the post-Variscan Late Carboniferous Auernig Group do not clearly correspond to a typical molasses deposit, as feldspar is lacking in modal analysis (Fontana and Venturini 1982; Krainer 1992). This absence of feldspars may be caused by humid climate conditions in the source region or by dissolution during sedimentary processes (e.g. transport, duration of deposition, diagenesis). The samples represent compositionally mature quartz-rich sandstones with high amounts of detrital white mica and rutile. The subangular grain shape of quartz suggests primary, first-cycle material from sedimentary and metamorphic sequences of a recycled orogenic source as indicated by the QFL diagram and the heavy mineral contents.

Detrital white mica were derived from high-pressure dominated metamorphic rocks (of the eroding Variscan orogen; Fig. 15) as seen in the high phengitic components, but without significant magmatic supply.

Permian

Early Permian samples, petrographically represented as quartz arenites or lithic arenites, display a similar provenance as the Late Carboniferous sandstones, indicating a craton interior source in QFL and a recycled orogenic source in Q_mFL_t plots, respectively. The Late Permian lithic greywacke points to a recycled orogen as the source area.

The average amount of detrital white mica is lower than in the Late Carboniferous sandstones. This distinct feature can be interpreted with regard to the above mentioned differentiation of post-orogenic molasse sediments and passive continental margin deposits.

The Permian samples are geochemically considered as litharenite, greywacke, arkose and shale, and, therefore, display a similar heterogeneous feature as the Late Carboniferous units and demonstrate a passive margin, continental island arc, and active continental margin as tectonic setting. The latter two settings may be due to the high Al_2O_3 and Fe_2O_3 contents in the matrix and framework constituents of some samples. The two contrasting settings may be explained by oblique rifting and bimodal magmatic activity that is proposed for the Central European Permian (Arthaud and Matte 1977; Muttoni et al. 1996; Stampfli et al. 2002). According to this, the patterns of the Permian samples, with their contrasting chemical and petrographic properties, indicate a rift setting (Fig. 15).

Mica composition of Late Permian successions demonstrate a low-grade metamorphic source. A plutonic source may be assumed for the Early Permian deposited micas, suggested by the high potassium contents, which are indicative for magmatic muscovites.

Comments on provenance study methods

In our study, some misfits between modal analysis and geochemical discrimination diagrams arose as well as the fact of strongly deviating chemical compositions plotting outside of proposed discrimination diagrams. Furthermore, important geodynamic settings are not discriminated in chemical discrimination diagrams, e.g. molasse versus passive continental margin settings.

The tectonic-setting-discrimination diagrams generally suggest a passive margin setting for the Late Carboniferous sandstones. Just as for petrographic diagrams, sandstones of molasse successions are not considered in chemical discrimination diagrams. However, the significant high amount of detrital white mica in most of the post-orogenic basins, which is reflected in chemical data by the potassium and aluminium contents, may be successfully used for the distinction of molasse-type basins from passive continental margin settings, as proposed by detrital mode analysis (Neubauer 1994). The geochemical and petrographic classifications of the Late Carboniferous sandstones are contradictory. Petrographically, most Late Carboniferous samples, are classified as sublitharenites and lithic arenites, whereas they are geochemically classified mainly as wacke and arkose. This geochemical difference is mainly attributed to the relatively high mica content in these samples, causing a shift into the arkose fields due to their lower SiO_2/Al_2O_3 and Na_2O/K_2O ratios. Therefore, the geochemical patterns in classification diagrams such as of Pettijohn et al. (1972) and Herron (1988) have to be interpreted with caution and should be thoroughly compared with the petrography, especially with respect to the post-orogenic nature of sediments and their high mica contents.

Unusual high contents on heavy minerals like rutile can result in misclassification using geochemical discrimination. Consequently, geochemical discrimination should be always based with inspection of thin sections, specifically when samples display unusual chemical compositions.

Also, detrital white micas were not considered in provenance analysis diagrams by the Gazzi–Dickinson method, although there are significant variations in different lithostratigraphic units as clearly indicated in Fig. 5. Park and Pilkey (1981), Potter (1994) and Neubauer (1994) discussed detrital white mica as a significant indicator of the geodynamic setting. As proposed by Neubauer (1994), detrital muscovites, which can contribute >20 vol% of the framework minerals in sandstones, can be a useful tool for the discrimination between passive margin sediments (<2 modal%) and post-orogenic molasse deposits (2–28%), but this still needs a larger data base from other orogens.

In addition, an informed consideration of white mica in detrital mode analysis may help to distinguish the geodynamic setting of the depositional basin in greater detail. We suggest that there is a relationship between the exhumation of middle crustal level of continental crust in late orogenic stages within collisional orogens (with mica-rich rocks such as mica-schists, gneiss and S-type granites) and the deposition of such mica-rich sandstones. This occurrence could be applied to monitor the geodynamic setting of the basin. For further provenance studies of clastic sediments in the Carnic Alps, and other regions, we suggest to take detrital white mica and its effect on geochemical and petrographic analyses into consideration in more detail. As detrital white mica is a common framework constituent in post-orogenic molasse-type sequences, it should not be neglected in provenance studies. Systematic and detailed studies of the influence of detrital phyllosilicates, as framework component and in the matrix, to geochemical and petrographic discrimination and classification will provide new and possibly important information in the provenance and tectonic setting analysis of terrigenous sedimentary rocks.

Antonitsch (1993) and Neubauer (1994) among others, point out that some plate tectonic settings, such as rift zones, are not considered in the classical ternary diagrams. Antonitsch (1993) interpreted similar plots that display an inconsistent feature of passive and active continental margin settings as continental rift environment due to the mixture of mature continental and mafic volcanic sources.

Whole-rock geochemical classification of the post-Variscan sandstones contrasts with classification from sandstone modal analysis due to the high amount of detrital white mica, which are conventionally excluded in quantitative petrographic analyses. The scatter of the samples in the chemical plots is largely due to the variable proportion of these detrital micas in the sand-size fraction in the various samples. Moreover, the matrix composition, which is not regarded in conventional detrital mode analysis either, also plays a significant role in the interpretation of geochemical data. Similarly, the geochemical classifications and discrimination diagrams used are not well suited for mica-rich siliciclastics, nor for sandstones rich in ultrastable heavy minerals. The influence of detrital white mica in sandstones is not commonly taken into account in interpreting provenance and tectonic setting from data of detrital mode and whole-rock geochemical analyses. Where sandstones contain abundant white mica, as in many Palaeozoic and Tertiary, post-orogenic molasses basins, the high mica content will significantly influence the geochemical discrimination plots.

Conclusions

Petrographical and geochemical data of sandstones from the Carnic Alps indicate Late Ordovician stable craton and recycled orogenic or extensional setting, Early Carboniferous compressional, Late Carboniferous foreland basin and Permian extensional geodynamic settings. Contrasting geochemical patterns of post-Variscan and Permian sequences are interpreted as rift settings. Thus, our results support existing geodynamic concepts of the

evolution of the Carnic Alps (e.g. Schönlaub and Heinisch 1993, with references).

For provenance studies, we recommend to use a multi-method approach including modal analysis and heavy mineral analysis rather than a purely geochemical approach. The present versions of chemical discrimination diagrams can yield good results, but need support by petrographic analysis, specifically when unusual compositions arise.

Beside the age information, both the proportion within framework constituents and the chemical composition of detrital white mica can give further clues to discrimination of the geodynamic settings and the composition of source.

Acknowledgements We acknowledge generous support by the Austrian Research Foundation FWF (grant no. P10506-GEO) to F.N. Dan Topa (Salzburg) helped with electron microprobe analysis. We thank Wolfgang Frisch (Tübingen) for remarks to an initial version of the manuscript, and Konrad Hammerschmidt (Berlin), Christoph Heubeck (Berlin), Juergen von Raumer (Fribourg), Igor Villa (Bern), Gian Gaspare Zuffa (Bologna) and an anonymous journal reviewer for thoughtful suggestions to an earlier version of the manuscript as well as for help to polish the final version.

References

Antonitsch W (1993) Die geologische Entwicklung in der zentralen Gurktaler Decke (Oberostalpin), Kärnten, am Beispiel der Kruckenspitze. MSc Thesis, University of Graz

Argast S, Donnelly TW (1987) The chemical discrimination of clastic sedimentary components. J Sediment Petrol 57:813–823

Arthaud F, Matte P (1977) Late Paleozoic strike-slip faulting in Southern Europe and northern Africa: results of a right-lateral shear zone between Appalachians and the Urals. Bull Geol Soc Am 88:1305–1320

Banfield JF, Eggleton RA (1989) Apatite replacement and REE mobilization, fractionation, and fixation during weathering. Clays Clay Minerals 37:113–127

Bauluz B, Mayayo MJ, Fernandez-Nieto C, Lopez JMG (2000) Geochemistry of Precambrian and Paleozoic siliciclastic rocks from the Iberian Range (NE Spain): implications for source-area weathering, sorting, provenance, and tectonic setting. Chem Geol 168:135–150

Bhatia MR (1983) Plate tectonics and geochemical composition of sandstones. J Geol 91:611–628

Bhatia M (1985) Rare earth element geochemistry of Australian Paleozoic graywackes and mudrocks: provenance and tectonic control. Sediment Geol 45:97–113

Bhatia MR, Crook KAW (1986) Trace element characteristics of graywackes and tectonic setting discrimination of sedimentary basins. Contrib Mineral Petrol 92:181–193

Blatt H, Middleton GV, Murray R (1980) Origin of sedimentary rocks. Prentice-Hall, Englewood Cliffs

Crook KAW (1974) Lithogenesis and geotectonics: the significance of compositional variations in flysch arenites (graywackes). In: Dott RH, Shaver RH (eds) Modern and ancient geosynclinal sedimentation. Soc Econ Paleontol Mineral Spec Publ 19:304–310

Dallmeyer RD, Neubauer F (1994) Cadomian $^{40}Ar/^{39}Ar$ apparent age spectra of detrital muscovites from the Eastern Alps. J Geol Soc Lond 151:591–598

Dickinson WR (1985) Interpreting provenance relations from detrital modes of sandstones. In: Zuffa GG (ed) Provenance of arenites. Reidel, Dordrecht, pp 333–362

Dickinson WR, Suczek CA (1979) Plate tectonics and sandstone compositions. Am Assoc Petrol Geol Bull 63:2164–2182

Dickinson WR, Beard LS, Brakenridge GR, Erjavec JL, Ferguson RC, Inman KF, Knepp R, Lindberg FA, Ryberg PT (1983) Provenance of North American Phanerozoic sandstones in relation to tectonic setting. Geol Soc Am Bull 94:222–235

Dott RH (1964) Wacke, graywacke and matrix: what approach to immature sandstone classification? J Sediment Petrol 34:625–632

Fenninger A, Stattegger K (1977) Schwermineraluntersuchungen in den oberkarbonen Auernig-Schichten des Garnitzenprofils (Naßfeld, Karnische Alpen). Verh Geol Bundesanst 1977:367–374

Finger F, Steyrer HP (1990) I-type granitoids as indicators of a late Palaeozoic convergent ocean–continent margin along the southern flank of the central European Variscan orogen. Geology 18:1207–1210

Fenninger A, Schönlaub HP, Holzer HL, Flajs G (1976) Zu den Basisbildungen der Auernigschichten in den Karnischen Alpen (Österreich). Verh Geol Bundesanst 1976:243–255

Floyd PA, Shail R, Leveridge BE, Franke W (1991) Geochemistry and provenance of Rhenohercynian synorogenic sandstones: implications for tectonic environment discrimination. In: Morton AC, Todd SP, Haughton PDW (eds) Developments in sedimentary provenance studies. Geol Soc Spec Publ 57:173–188

Flügel HW (1975) Einige Probleme des Variszikums von Neo-Europa. Geol Rundsch 64:1–62

Fontana D, Venturini C (1982) Evoluzione delle mode detritiche nelle areanarie Permocarbonifere del bacino tardo-ercinico di Pramollo (Alpi Carniche). Mem Soc Geol It 33:43–49

Fralick PW, Kronberg BI (1997) Geochemical discrimination of clastic sedimentary rock sources. Sediment Geol 113:111–124

Franke W (1989) Tectonostratigraphic units in the Variscan belt of central Europe. Geol Soc Am Spec Pap 290:67–89

Frisch W, Neubauer F (1989) Pre-Alpine terranes and tectonic zoning in the Eastern Alps. Geol Soc Am Spec Pap 230:91–99

Herron MM (1988) Geochemical classification of terrigenous sands and shales from core or log data. J Sediment Petrol 58(5):820–829

Hinderer M (1992) Die vulkanoklastische Fleonsformation in den westlichen Karnischen Alpen- Sedimentologie, Petrographie und Geochemie. Jb Geol Bundesanst 135:335–379

Ingersoll RV, Bullard TF, Ford RL, Grimm JP, Pickle JD, Sares SW (1984) The effect of grain size on detrital modes: a test of the Gazzi–Dickinson point-counting method. J Sediment Petrol 54:103–116

Johnsson MJ (1993) The system controlling the composition of clastic sediments. In: Johnsson MJ, Basu A (eds) Processes controlling the composition of clastic sediments. Geol Soc Am Spec Pap 284:1–19

Krainer K (1992) Fazies, Sedimentationsprozesse und Paläogeographie im Karbon der Ost- und Südalpen. Jb Geol Bundesanst 135(1):99–193

Krainer K (1993) Late- and Post-Variscan sediments of the Eastern and Southern Alps. In: von Raumer JF, Neubauer F (eds) Pre-Mesozoic geology in the Alps. Springer, Berlin Heidelberg New York, pp 537–564

Läufer A, Loeschke J, Vianden B (1993) Die Dimon-Serie der Karnischen Alpen (Italien)-Stratigraphie, Petrographie und geodynamische Interpretation. Jb Geol Bundesanst 136:137–162

Läufer AL, Hubich D, Loeschke J (2001) Variscan geodynamic evolution of the Carnic Alps (Austria/Italy). Int J Earth Sci 90:855–870

Mader D, Neubauer F, Handler R (2000) Palaeozoic sandstones in the Carnic Alps (Austria): geodynamic setting by geochemistry, detrital mode and $^{40}Ar/^{39}Ar$ dating. Mitt Ges Geol Bergbaustud Österr 43:89–90

McBride EF (1963) Diagenetic processes that affect provenance determinations in sandstone In: Zuffa GG (ed) Provenance of arenites. Reidel, Dordrecht, pp 95–114

McLennan SM (1989) Rare earth elements in sedimentary rocks: influence of provenance and sedimentary processes. In: Lipin BR, McKay GA (eds) Geochemistry and mineralogy of rare earth elements. Mineral Soc Am 21:169–200

McLennan SM, Taylor SR, McCulloch MT, Maynard JB (1990) Geochemical and Nd–Sr isotopic composition of deep-sea turbidites: crustal evolution and plate tectonic associations. Geochim Cosmochim Acta 54:2015–2050

McLennan SM, Hemming S, McDaniel DK, Hanson GN (1993) Geochemical approaches to sedimentation, provenance, and tectonics. In: Johnsson MJ, Basu A (eds) Processes controlling the composition of clastic sediments. Geol Soc Am Spec Pap 284:21–40

Morey GB, Setterholm DR (1997) Rare earth elements in weathering profiles and sediments of Minnesota: implications for provenance studies. J Sediment Res 67:105–115

Muttoni G, Kent D, Channel JET (1996) Evolution of Pangaea: palaeomagnetic constraints from the Southern Alps, Italy. Earth Planet Sci Lett 140:97–112

Nesbitt HW (1979) Mobility and fractionation of rare earth elements during weathering of a granodiorite. Nature 279: 206–210

Nesbitt HW, MacRae ND, Kronberg BI (1990) Amazon deep-sea fan muds: light REE enriched products of extreme chemical weathering. Earth Planet Sci Lett 100:118–123

Neubauer F (1994) Geodynamic significance of Palaeozoic sandstones in the Eastern Alps. J Czech Geol Soc 39:76–77

Neubauer F, Handler R (2000) Variscan orogeny in the Eastern Alps and Bohemian Massif: how do these units correlate? Mitt Österr Geol Ges 92(1999):35–59

Neubauer F, Sassi FP (1993) The Austro-Alpine quartzphyllites and related Palaeozoic Formations. In: von Raumer JF, Neubauer F (eds) Pre-Mesozoic geology in the Alps. Springer, Berlin Heidelberg New York, pp 423–439

Neubauer F, Klötzli U, Poscheschnik P (2001) Cadomian magmatism in the Alps recorded in Late Ordovician sandstones of the Carnic Alps: preliminary results from zircon Pb/Pb evaporation dating. Schweiz Mineral Petrogr Mitt 81:175–179

Park YA, Pilkey OH (1981) Detrital mica: environmental significance of roundness and grain surface textures. J Sediment Petrol 51:113–120

Pettijohn FJ, Potter PE, Siever R (1972) Sand and sandstone. Springer, Berlin Heidelberg New York

Pettijohn FJ, Potter PE, Siever R (1987) Sand and sandstone, 2nd edn. Springer, Berlin Heidelberg New York

Poscheschnik P (1993) Stratigraphy, sedimentology and sandstone composition of clastic Late Ordovician sequences from the Carnic Alps (Austria, Italy). MSc Thesis, University of Graz

Potter PE (1994) Modern sands of South America: composition, provenance and global significance. Geol Rundsch 83:212–232

Roser BP, Korsch RJ (1986) Determination of tectonic setting of sandstone-mudstone suites using SiO_2 content and K_2O/Na_2O ratio. J Geol 94:635–650

Schnabel W (1976) Schwermineraluntersuchungen im Variszikum der Karnischen Alpen (Österreich und Italien). Verh Geol Bundesanst 1979:A154–A155

Schönlaub HP (1985a) Das Paläozoikum der Karnischen Alpen. Führer zur Arbeitstagung der Geologischen Bundesanstalt, Kötschach-Mauthen, Gailtal. Geologische Bundesanstalt, Wien

Schönlaub HP (1985b) Geologische Karte der Republik Österreich 1:50 000, 197 Kötschach. Geologische Bundesanstalt, Wien

Schönlaub HP (1987) Geologische Karte der Republik Österreich 1:50 000, 198 Weissbriach. Geologische Bundesanstalt, Wien

Schönlaub HP, Heinisch H (1993) The classic fossiliferous Palaeozoic units of the Eastern Alps. In: von Raumer J F, Neubauer F (eds) Pre-Mesozoic geology in the Alps. Springer, Berlin Heidelberg New York, pp 395–422

Schönlaub HP, Histon K (2000) The Palaeozoic evolution of the Southern Alps. Mitt Österr Geol Ges 92 (1999):15–34

Schwab (1975) Framework mineralogy and chemical composition of continental margin-type sandstones. Geology 3:487–490

Spalletta C, Venturini C (1988) Conglomeratic sequences in the Hochwipfel Group: a new palaeogeographic hypothesis on the Hercynian flysch stage of the Carnic Alps. Jb Geol Bundesanst 131:637–647

Spalletta C, Vai GB, Venturini C (1980) Il flysch ercinico nella geologia die Monti Paularo e Dimon (Alpi Carniche). Mem Soc Geol It 20:243–265

Spear FS (1993) Metamorphic phase equilibria and pressure-temperature–time paths. Mineral Soc Am, Washington, DC

Speer JA (1984) Micas in igneous rocks. In: Bailey SW (ed) Micas. Rev Mineral. Mineral Soc Am, Washington, DC, pp 299–356

Stampfli GM, von Raumer J, Borel G (2002) The Paleozoic evolution of pre-Variscan terranes: from Gondwana to Variscan collision. Geol Soc Am Spec Pap 364:263–280

Taylor SR, McLennan SH (1985) The continental crust: its composition and evolution. Blackwell, Oxford

Tietz GF (1974) Die Schwermineralgehalte in den Grenzlandbänken (Unterperm der Karnischen Alpen, Standardprofil Rattendorfer Sattel). Carinthia II 164/84:115–124

Tollmann A (1985) Der südalpine Anteil Österreichs. Geologie von Österreich, Band 2, Außerzentralalpiner Anteil, Deuticke, Wien, pp 240–300

Toulkeridis T, Clauer N, Kröner A, Reimer T, Todt W (1999) Characterization, provenance, and tectonic setting of Fig Tree greywackes from the Archean Barberton Greenstone Belt, South Africa. Sediment Geol 124:113–129

Valloni R, Zuffa, GG (1984) Provenance changes for arenaceous formations of the northern Apennines, Italy. Geol Soc Am Bull 95:1035–1039

Venturini C (ed) (1990a) Field workshop on Carboniferous to Permian sequence of the Pramollo–Nassfeld Basin (Carnic Alps). 2–8 September 1990, Guidebook, Udine

Venturini C (1990b) Geologia delle Alpi Carniche Centro Orientali. Comune di Udine, Mus Friulano Storia Naturale 36

von Raumer JF (1998) The Paleozoic evolution in the Alps: from Gondwana to Pangea. Geol Rundsch 87:407–435

Williams H, Turner FJ, Gilbert CM (1953): Petrography. Freeman, San Francisco

Zhang L, Sun M, Wang S, Yu X (1998) The composition of shales from the Ordos basin, China: effects of source weathering and diagenesis. Sediment Geol 116:129–141